Enhanced methane cycling across the Laptev Sea signaled by time-integrated biomarkers of aerobic methane oxidation

Albin Eriksson[1,2], Birgit Wild[1,2], Wei-Li Hong[2,3,4], Henry Holmstrand[1], Francisco J.A Nascimento[4,5], Stefano Bonaglia[6], Denis Kosmach[7], Igor Semiletov[7,8,9], Natalia Shakhova[8,10], and Örjan Gustafsson[1,2]

[1] Department of Environmental Science (ACES), Stockholm University, Stockholm, Sweden
[2] Bolin Centre for Climate Research, Stockholm, Sweden
[3] Department of Geological Sciences (IGV), Stockholm University, Stockholm, Sweden
[4] Baltic Sea Centre, Stockholm University, Stockholm, Sweden
[5] Department of Ecology, Environment and Plant Sciences, Stockholm University, Stockholm, Sweden
[6] Department of Marine Sciences, University of Gothenburg, Gothenburg, Sweden
[7] Laboratory for Arctic Research, V.I. Ilichov Pacific Oceanological Institute (POI), Far Eastern Branch of the Russian Academy of Sciences, Vladivostok, Russia
[8] Laboratory for Integrated Research of the Arctic System "land-shelf", National Tomsk State Research University (TSU), Tomsk, Russia
[9] Laboratory of Chemical and Biological Research, Sakhalin State University (SakhSU), Yuzhno-Sakhalinsk, Russia
[10] Sadovsky Institute of Geosphere Dynamics (IGD) of the Russian Academy of Sciences, Moscow, Russia

Correspondence to: Albin Eriksson (albin.eriksson@aces.su.se) and Örjan Gustafsson (orjan.gustafsson@aces.su.se)

Abstract. Elevated methane concentrations in seawater have been reported over extensive areas of the East Siberian Arctic Seas, overlying thawing subsea permafrost. However, observed methane concentrations of the ephemeral seawater are highly variable across both space and time, compromised by both the timing of rare measurements and storm-driven exchanges to the atmosphere. Here, we applied time-integrated signals of the $\delta^{13}C$-composition of specific C_{30} hopanoids (diploptene, hop-17(21)-ene, neohop-13(18)-ene and diplopterol) in surface sediments to trace aerobic methane oxidation as a proxy for enhanced methane cycling. Interpretations of hopanoids and possible sources were further assessed by 16S-rRNA analyses in the surface sediments. The consistently low $\delta^{13}C$-C_{30} hopenes signals, ranging between -57.5 to -37.1 ‰ (n=23) across the Laptev Sea shelf indicated aerobic methane oxidation. This suggests ubiquitous methane cycling with the most pronounced intensities in the outer shelf region, broadly consistent with the observed methane concentrations. Notably, depleted $\delta^{13}C$-C_{30} hopenes were also found in the mid-shelf region of the Laptev Sea, earlier thought to be an area of comparatively low methane cycling. High methane concentrations were also observed in the vicinity of the Lena River delta, yet the isotopically heavier $\delta^{13}C$-C_{30} hopenes may here reflect a combination of lower aerobic methane oxidation, a greater relative abundance of type II methanotrophs (lower isotope fractionation during hopanoid production) and isotope dilution from non-methanotrophic sources. While this complicates the biomarker interpretation in the unique setting near the Lena River delta, the $\delta^{13}C$-C_{30} hopenes were still much lower than $\delta^{13}C$-organic carbon, indicating aerobic methane oxidation and a clear methane cycling signal also in this regime. Taken together, the results unravel the wider cross-shelf patterns of enhanced methane cycling in the Laptev Sea through probing of methane fossilised in membrane lipids of aerobic methanotrophs, with the molecular-isotopic pattern being preserved in the sedimentary archive.

1 Introduction

Large uncertainties remain regarding methane (CH_4) emissions from both anthropogenic and natural systems (Saunois et al., 2025 Schaeffer et al., 2025). Terrestrial permafrost stores massive amounts of carbon, but climate change and Arctic amplification have enhanced its thawing, causing net CH_4 emissions to the atmosphere (Ramage et al., 2024; Hugelius et al., 2024). Subsea permafrost, formed from the inundation of the northern tundra during the last deglaciation, is often overlooked. Partly due to its inaccessibility, limiting the number of observations. However, observations display highly elevated CH_4 concentrations in the shallow seawater column overlying subsea permafrost (e.g., Semiletov, 1999; Shakhova et al., 2010; Steinbach et al., 2021), which is currently thawing about ten times faster than nearby terrestrial permafrost in Northeastern Siberia (Shakhova et al., 2017; Wild et al., 2022).

The East Siberian Arctic Shelf (ESAS), the world's largest continental shelf sea, is very shallow (on average, ca. 50 m) and estimated to host the majority of the world's subsea permafrost (Romanovskii et al., 2001; Romanovskii et al., 2005; Overduin et al., 2019). The concentration of CH_4 in the surface waters of the ESAS is, particularly in the Laptev Sea, much higher than what would be expected from CH_4 levels in the atmospheric boundary layer, suggesting that the thawing subsea permafrost system may serve as a conduit for CH_4 release to the atmosphere (Shakhova et al., 2010, 2014, 2019). A key challenge to constrain the geospatial pattern of CH_4 releases is the short-term variability of water column CH_4 concentrations, together with the sparseness of observations over time in this remote region. While subsea permafrost thaw and related CH_4 emissions are governed by environmental changes on decadal time-scales (Shakhova et al., 2017, 2019), the sparse and infrequent measurements of water column CH_4 concentrations might capture neither temporal nor geospatial trends of CH_4 emissions from these systems. Water sampling has revealed the general pattern of elevated CH_4 concentrations and discovered a few major hotspots, but this pattern is strongly affected by short-term variability governed by storms and the shallow water column of the Laptev Sea (e.g., Shakhova et al., 2014). Furthermore, a recent modeling study concluded that current atmospheric observation networks are not able to detect abrupt CH_4 releases from this region (Wittig et al., 2024). To better grasp the CH_4 dynamics over a longer timespan than what is captured in snapshot seawater samples, there is a need for an integrated metric to observe patterns of long-term CH_4 release from the subsea permafrost system over both space and time scales.

Specific biomarkers in surface sediments offer an opportunity to study large-scale variabilities in CH_4 and its dynamics integrated over time scales of years to decades. Bacteria in oxygenated sediments and in the water column can utilize CH_4 as an energy and carbon source through aerobic CH_4 oxidation (AeOM), converting it to carbon dioxide (CO_2; Hanson & Hanson, 1996), or assimilating it into biomass (e.g., lipid synthesis). Hopanoid lipids such as diploptene and diplopterol are important constituents of the cell membranes of Methane Oxidizing Bacteria (MOB) carrying out these processes (Summons et al., 1994), but can also derive from bacteriohopanepolyols (BHPs) upon diagenesis (Mackenzie et al., 1981). Hopanoids and BHPs are not only produced by MOB, but can stem from a variety of aerobic and anaerobic bacteria utilizing CH_4 and/or

inorganic/organic carbon (Rohmer et al., 1980; Summons et al., 1999; Sinninghe Damsté et al., 2004; Belin et al., 2018). Thus, hopanoid analyses are frequently combined with compound-specific isotope analysis of stable carbon isotopes ($\delta^{13}C$) to relate these biomarkers to CH_4 cycling. The isotopically depleted stable carbon isotopes of CH_4 $\delta^{13}C$-CH_4 (as low as -90 ‰; Milkov & Etiope, 2018) is used to differentiate CH_4-derived hopanoids from other sources. Thereby, C_{30}-hopanoids (hopanoids with 30 carbon atoms) have been used as a proxy to infer enhanced CH_4 cycling in past climates (e.g., Hinrichs, 2001; Hinrichs et al., 2003; Birgel and Peckmann, 2008; Sun et al., 2022; Blumenberg et al., 2024; Yan et al., 2025) and contemporary systems (Davies et al., 2016; Inglis et al., 2019). Generally, enhanced CH_4 cycling has been linked to decreasing $\delta^{13}C$ values of hopanoids (e.g., Inglis et al., 2019; van Winden et al., 2020; Yan et al., 2025). Therefore, $\delta^{13}C$-hopanoids may be used as a time-integrated signal of enhanced CH_4 cycling. In particular, hopanoid carbon chain lengths $\leq C_{30}$ are often more depleted in ^{13}C compared to C_{31}-hopanoids and therefore closely associated with MOB production of hopanoids (Inglis et al., 2019). While the proxy has been widely used to study CH_4 dynamics in past climates, contemporary system calibrations of $\leq C_{30}$ hopanoids only exist in peatlands ($\leq C_{30}$ hopanoids between -21 and -45 ‰; Inglis et al., 2019) and lacustrine systems (diploptene ranging from -38.8 to -68.8‰; Davies et al., 2016). The lack of a large-scale comparison of CH_4 and hopanoids in marine systems leaves uncertainties when interpreting $\delta^{13}C$-hopanoids as tracers of CH_4 cycling in geological records. In summary, $\delta^{13}C$-hopanoids in oxygenated surface sediments can be an informative tool to constrain a time-integrated signal of enhanced CH_4 cycling on a years-decade scale, complementing observations of CH_4 concentrations in seawater which is highly variable over much shorter time-scales.

Observations across the Laptev Sea suggest the presence of AeOM, but its efficiency is questionable and spatially variable. The Laptev Sea water and surface sediments are well oxygenated (Stepanova et al., 2017; Brüchert et al., 2018; Maciute et al., 2025), with the water column oxygen saturation ranging from 70-100% during expeditions between 2015 and 2020 (Xie et al., 2023). This combined with high CH_4 concentrations, indicates the general possibility for AeOM. Furthermore, microbial studies have confirmed the presence of MOB in Laptev Sea sediments and water column (Samylina et al., 2021; Savvichev et al., 2023). Recent machine-learning estimations deemed the global AeOM to be generally efficient in coastal waters (Mao et al., 2022), but AeOM observations in the vicinity of the Lena River delta display a rather weak methanotrophic sink, with a CH_4 turnover time of 193 days in mixed sea/river water (Bussmann et al., 2017). In contrast, incubation experiments in the outer Laptev Sea cold seep region suggest more efficient AeOM in those surface sediments (Tikhonova et al., 2021), but with very low AeOM rates in the water column (300-1000 days turnover time, Shakhova et al., 2015). Taken together, AeOM is active in the Laptev Sea, but observations are diverging on the scale and efficiency of AeOM across the Laptev Sea. Such discrepancies highlight the importance of constraining the geospatial distribution of AeOM to unravel areas of more intense CH_4 cycling.

In this study, we explore AeOM biomarkers as time-integrated proxies of CH_4 cycling in Arctic Ocean water and sediments, focusing on the Laptev Sea. We hypothesize that known CH_4 ebullition hotspots in the Outer Laptev Sea and Inner Laptev Sea

(OLS and ILS), where >1000 nM dissolved CH_4 concentrations have been observed (Shakhova et al., 2010, 2014; Steinbach et al., 2021), have high concentrations of AeOM-tracing C_{30} hopanoids (diploptene, hop-17(21)-ene, neohop-13(18)-ene and diplopterol) with low $\delta^{13}C$ values. In contrast, we hypothesize that the mid-shelf region without any discovered CH_4 hotspots, yet with dissolved CH_4 concentrations in the range 10-60 nM (Fig.2) display lower concentrations of C_{30} hopanoids more enriched in ^{13}C. Observations of AeOM biomarkers are also compared to water CH_4 concentrations and 16S-rRNA data on abundance of MOB- and non-methanotrophic hopanoid-producing bacteria. We finally use this dataset to explore the geospatial distribution of CH_4 cycling across the 600 km wide Laptev Sea shelf. Insights from this study also allows to establish some general considerations for interpreting hopanoids in geological records.

2 Methods

2.1 Study area and the ISSS-2020 expedition

During the last deglaciation, sea level rise caused the northern regions of East Siberian permafrost to be submerged, thus forming the present coverage of Laptev Sea subsea permafrost (Romanovskii et al., 2001; Romanovskii et al., 2005; Nicolsky & Shakhova, 2010; Shakhova et al., 2017; Lindgren et al., 2018; Overduin et al., 2019). The Laptev Sea water column is shallow (average water depth ~50 m), with well oxygenated top mm to cm of surface sediments (Brüchert et al., 2018; Maciute et al., 2025). Ebullition appears to be a key transport vector in this shallow region, transferring large amounts of CH_4 to the water column (Shakhova et al., 2010, 2014; Steinbach et al., 2021). The Inner (ILS; latitudes < 73.9°N & longitudes ~130°E) and Outer Laptev Sea hotspot regions (OLS; latitudes ≥ 76.1°N & longitudes 125-131°E) are established as areas of extensive CH_4 cycling in the water column, with their shallowness causing frequent ventilation of the water column CH_4 to the overlying atmosphere (e.g., Shakhova et al., 2010, 2014; Thornton et al., 2016, 2020; Steinbach et al., 2021; Chernykh et al., 2023). Results from campaigns of subsea permafrost drilling have indicated rapid thawing of subsea permafrost in the ILS region (e.g., Shakhova et al., 2017). Thawing subsea permafrost is considered to facilitate CH_4 release from the very shallow ILS (Shakhova et al., 2014; Sapart et al., 2017; Wild et al., 2022). In the deeper, yet still shallow OLS (46-72 m), a thermogenic gas reservoir has been constrained as the main CH_4 source using triple isotope fingerprinting (Steinbach et al., 2021). The Laptev Sea is also strongly influenced by the Lena River plume (Shakhova & Semiletov, 2007; Shakhova et al., 2010). While the ILS receives substantial amounts of organic carbon from the Lena River (Vonk et al., 2012; Holmes et al., 2012; McClelland et al., 2016; Bröder et al., 2018; Martens et al., 2022), the riverine export of CH_4 is negligible in comparison to the regional CH_4 emissions (Shakhova & Semiletov, 2007; Shakhova et al., 2010). The mid-outer Laptev Sea transect (MLS; latitudes between 73.9-76.1°N & longitudes ~130°E) is, in contrast, an area of lower CH_4 concentrations than the ILS and OLS, yet the still elevated CH_4 levels over extensive MLS scales (Shakhova et al., 2010) call for investigations on potential CH_4 sources also for this region. Samples in the current study were collected from the Laptev Sea during the International Siberian Shelf Study in 2020 (ISSS-2020; Sept- Nov. 2020) aboard the research vessel *Akademik Keldysh* (Fig.1).
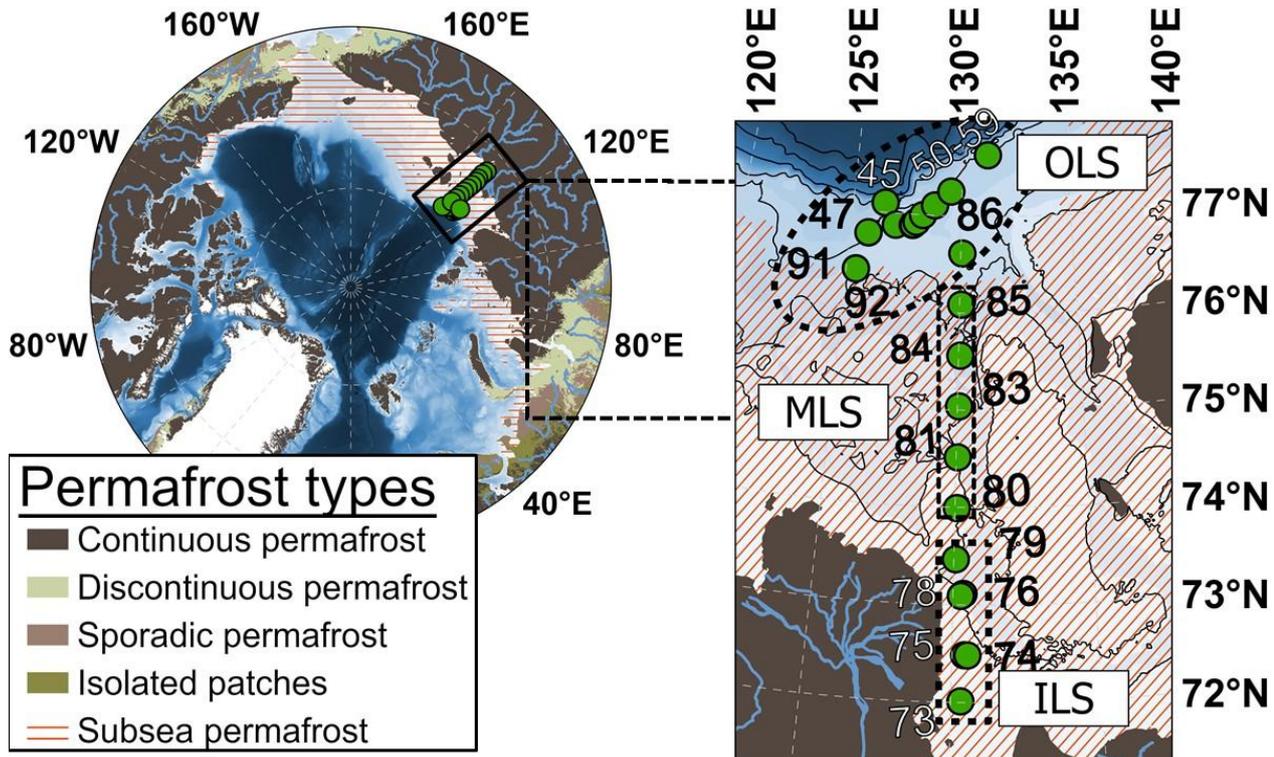
Figure 1. The Laptev Sea sampling locations and station numbers, including estimates of the current Arctic land and subsea permafrost covers. Permafrost datasets were generated from Obu et al. (2019) and Overduin et al. (2019). The bathymetry was plotted using IBCAO version 5.0 (Jakobsson et al., 2024).

2.2 Sediment and Water Sampling

2.2.1 Sediment sampling

Sediment samples were retrieved using an Oktopus Multicorer System that sampled eight cores per station with an undisturbed sediment-water interface. The penetration depth of the liners was a maximum of 30 cm. Overlying water was drained off the surface sediment in the cores and the sediment was subsequently sectioned in 1 cm intervals onboard using an Oktopus Core Extruder. All sediment subsamples for organic geochemical analyses were immediately frozen in plastic seal bags and the 1-2 cm slice in each core was used to extract lipid biomarkers for this study.

Sediment cores with pre-drilled holes on the liners were collected for 16S-rRNA analysis at n=36 stations (Maciute et al., 2025), where n=11 samples from the Laptev Sea shelf were used in this study. The overlying water was siphoned from the top of the sediment core and 3 ml of sediment was subsampled from three sampling depths in the core (0-1.5 cm, 1.5-3 cm, & 3-4.5 cm). Subsamples were vortexed with 10 ml RNA*later* (Sigma Aldrich) and stored for 2 h at 4°C before being frozen at -

80℃. In this study, we only report the top 0-1.5 cm subsection for microbial analyses, as the focus was on aerobic CH_4 oxidizers.

2.2.2 Measurements of dissolved methane concentration in the water column

155   Water samples were taken from a Rosette sampler with 24 x 10 L bottles, closed at selected depths. Subsamples were immediately taken through silicon tubes into 60 ml Luer-lock plastic syringes for onboard CH_4 concentration measurements. Briefly, a Restek reservoir bag was used for helium headspace equilibration with an IKA KS 260 benchtop shaker. Before concentration measurements using Gas Chromatography-Flame Ionization Detection (GC-FID), the gases were transferred through stainless-steel Millipore filter holders packed with granular Drierite and quartz wool, sealed using PTFE tape. The

160   CH_4 concentration measurements were made with 5 ml sample injections through one 1/8" Porapak Q packed pre-column and a 3 m 1/8" Heyesep D column before FID. In this study, the surface water is described as the topmost CTD/Rosette-based water samples (mean =3.5 m; n=21) and the sub-pycnocline (mean =37 m; n =71) as water samples below the largest density gradient (σ_θ) based on the CTD profile (Conductivity, Temperature and Depth). The sub-pycnocline concentrations are here reported as the median and interquartile ranges of all samples between the pycnocline and the bottom water (Fig. 2).

2.3 Measurements of methane-tracing lipid biomarkers and their isotope composition

165   Bulk organic carbon and stable carbon isotope (δ^{13}C-OC) analyses of the 1-2 cm slice in each multicore were made according to standard operating procedures at Stockholm University (e.g., Martens et al., 2020). Briefly, ~10 mg freeze-dried sediment was weighed in silver capsules and acidified with 100 µl 1M HCl twice for the removal of inorganic carbon. After the first acidification, the sample was stored at 50℃ for 3-4 hours, followed by acidification again and reaction at 50℃ overnight. The

170   acidified samples were wrapped in tin capsules and analysed with an elemental analyser coupled to an isotope ratio mass spectrometer (EA-irMS, Delta V Plus, Thermo Scientific, Germany).

2.3.1 Lipid extraction

Around 5 g of freeze-dried sediment was subsampled from one core per station. Before the extractions, internal standards were added to each sample (5α-androstane, tetracosane-d_{50}, triacontane-d_{62}, eicosanoic acid-d_{39}, 2-hexadecanol and stigmasterol-d_5)

175   to calculate recoveries and correct for losses during the laboratory procedure. The lipid extraction and clean-up were a modification of standard operating procedures at Stockholm University (e.g., van Dongen et al., 2008; Vonk et al., 2012; Martens et al., 2020). Briefly, lipids were extracted using accelerated solvent extraction (ASE 350, Dionex), followed by elemental sulphur and water removal from the extracts by addition of HCl-activated Cu and anhydrous $NaSO_4$. The total lipid extracts were saponified for 2 h at 80℃ following the addition of ~3 ml KOH (6 % in MeOH) to each of the dried samples.

180   Base-catalysed hydrolysis was applied as it has been shown to increase the amount of hopenes through dehydration of diplopterol (Sessions et al., 2013). The saponified neutral lipids (containing hopanoids, alkanes, sterols and alkenones) were collected with liquid-liquid extraction five times with the addition of 1 ml Milli-Q water and ~2 ml hexane: DCM (9:1, v/v).

After collecting the neutral fraction, the saponified sample was acidified to pH 1 with 6 M HCl, ~2 ml hexane: DCM (9:1, v/v) was added, the sample was mixed and the supernatant containing the fatty acid fraction was collected. The fatty acid liquid-liquid extraction was repeated five times in total. In this study, we focused on the neutral fraction, containing hopanes/hopenes/diplopterol.

Following the saponification and separation of the neutral and fatty acid fractions, preparative chromatography was applied to the neutral fraction, with furnace-baked alkaline Al_2O_3 (~0.5 g) in a pre-combusted Pasteur pipette as the stationary phase. The neutral fraction was separated into non-polar hydrocarbons (hopanes/hopenes, F1), alkenones/diplopterol (F2) and polar hydrocarbons (F3) using 4 ml hexane: DCM (9:1, v/v), hexane: DCM (1:1) and DCM: MeOH (1:1, v/v), respectively. To enable clean chromatograms for $\delta^{13}C$ measurements, urea adduction was applied to purify the non-polar extracts (Pancost et al., 2008; Inglis et al., 2019). The sample was separated into an adduct (containing *n*-alkanes) and a non-adduct fraction (containing cyclic and branched hydrocarbons, e.g., hopenes). Before instrument analysis, the diplopterol fraction was silylated for 1h at 80°C using BSTFA: pyridine (1:1).

2.3.2 Hopanoid identification and quantification

Hopanoids were quantified using gas chromatography-mass spectrometry (GC-MS 7820-A, Agilent Technologies USA) with a DB5-MS ultra-inert column (30 m x 250 µm x 0.25 µm). The GC-MS was run in splitless mode with a starting temperature of 50°C for 2 min, then 10 °C/min to 210°C, where the temperature increased by 3°C/min to 262°C for 10 min. Thereafter, the temperature increased by 0.5°C/min to 270∘C and lastly a 3°C/min ramp until 310°C for 5 min. A post-run at 305°C for 2 min was used to minimize sample carryover. Identification of hopanoids was done according to published mass spectra in Sessions et al. (2013), Sinninghe Damsté et al. (2014) and Elvert & Niemann, (2008). Hopenes were quantified using the C_{30} hopane external calibration standard (NIST 2266). However, during sample pre-treatment, dehydration of diplopterol and subsequent conversion to diploptene and hop-21-ene were observed within F2. This was likely catalysed by the basic Al_2O_3 column, as the problem resolved when switching to neutral Al_2O_3, which was used to separate the molecules before the final analysis. Diplopterol dehydration commonly occurs during sample workup, even during instrumental analysis (Kannenberg et al., 1995; Sessions et al., 2013). Thus, in this paper, we only present the $\delta^{13}C$ value of diplopterol when possible and not its concentrations.

2.3.3 Compound-specific isotope analysis of hopanoids

Compound-specific isotope analysis (CSIA) of hopenes/diplopterol was carried out at Stockholm University using gas chromatography coupled to continuous flow isotope ratio mass spectrometry (GC-irMS; Trace-GC, GC-Isolink and Delta V Plus, Thermo Scientific, Germany) on a DB5-MS ultra-inert column (60 m x 0.25 mm x 0.25 µm). The oven temperature program was the same as for GC-MS analyses. Briefly, triplicate 3 µl injections were made for each sample and quantified using external *n*-alkane standards (n-alkane mixture A7, Dr. Arndt Schindelmann, Indiana University). Before each batch of

215   sample measurements, the precision and linearity of *n*-alkane standards were monitored to ensure precision ≤ 0.5 ‰ (n =6). The reproducibility of triplicate sample measurements was 0.1-2.3 ‰ (mean= 0.8 ‰). The higher standard deviations of some samples were attributed to lower peak areas, causing less precise measurements. To minimize the precision effect from lower peak areas, an acceptance threshold of ≥100 mV peak areas was set, at which *n*-alkane standard measurements yielded a precision of 0.9 ‰. The added trimethylsilyl (TMS; Si-(CH$_3$)$_3$) in δ^{13}C measurements was corrected by measuring a silylated

220   β-sitosterol standard using GC-irMS and the unsilylated β-sitosterol powder with EA-irMS. The difference in δ^{13}C between the silylated and unsilylated standard was used as the δ^{13}C of the added carbon to derivatized compounds, where f is the fraction of added carbon from the TMS group and δ^{13}C$_{TMS}$ is the isotopic value of the TMS (Eq. 1).

$$\delta^{13}C_{Diplopterol} = \frac{(\delta^{13}C_{Silylated\ diplopterol} - f*\delta^{13}C_{TMS})}{(1-f)} \tag{1}$$

2.4 Microbiology

225 **2.4.1 DNA extraction and sequencing**

Sediment samples were thawed and prepared to facilitate 16S-rRNA analyses as described in Maciute et al. (2025). Extractions were made from 2.9±0.7g wet sediment and amplification of the 16S rRNA gene V4 region was conducted with the primers 515 F (Parada et al., 2016) and 806 R (Apprill et al., 2015). Library preparation was conducted using the NEBNext® Ultra™ II DNA Library Prep Kit with index adapters synthesized in-house by Novogene. The pooled library was sequenced on the

230   Illumina NovaSeq 6000 SP platform with a 2x250 bp paired-end setup. The raw sequencing data have been uploaded to NCBI GenBank (https://www.ncbi.nlm.nih.gov/bioproject/) and can be accessed at BioProject: PRJNA1264051.

2.4.2 Bioinformatics

A total of 2,341,395 million sequencing reads, averaging 65 039 reads per sample (36 samples in total) were analysed according to the DADA2 (version 1.28) pipeline (Callahan et al., 2016) with default settings except for the filter commands:

235   truncLen=c(0,0), maxEE=2, truncQ=2, trimLeft=c(22,21); error model: MAX_CONSIST = 30; merging of pair-ends: minOverlap=10; and chimera removal: allowOneOff=TRUE, minFoldParentOverAbundance=4. After trimming, filtering, merging pair-ends and chimera removal, a total of 89,148 amplicon sequence variants and 9.2 million sequences were retained, averaging 43,485 reads per sample (minimum 26,424 and maximum 66,969 reads per sample). The sequences in the created ASV table were then assigned to taxonomy using the SILVA database version 132 (Quast et al., 2013) and analysed further as

240   relative abundances (i.e., [counts/∑counts] × 100) in RStudio software. Only the samples collected and sequenced from the Laptev Sea shelf are discussed in this study (n = 11).

2.4.3 Relative abundance of methane-oxidizing bacteria and non-methanotrophic hopanoid producers

Microbial sequencing data were explored for both aerobic methanotrophs as well as other hopanoid-producing bacteria. Aerobic methanotrophs were identified within *Gammaproteobacteria* (Type I) and *Alphaproteobacteria* (Type II). Bacteria within phyla that commonly encode *shc* (squalene-hopane cyclases, i.e., hopanoid producers), such as *Cyanobacteria,* were assumed to be hopanoid producers. Literature exploration of other organisms with documented production of hopanoids was made using LOTUS (Rutz et al., 2022) and was further used to assess "Other hopanoid producers". Particularly, the abundance of certain *Acidobacteria*, *Actinobacteria* and non-methanotrophic *Proteobacteria* described in previous research of hopanoid producers (Sohlenkamp & Geiger, 2016; Sinninghe Damsté et al., 2017) was used to explore non-methanotrophic hopanoid producers. The information on all investigated hopanoid producers can be found in the supplementary data (Data availability).

2.5 Statistical analyses

Statistical differences were evaluated using a significance level $\alpha=0.05$ in RStudio (Version 2024.12.1). One-way Welch's ANOVAs were applied to analyse differences in hopanoid concentrations and isotope signatures between the OLS, MLS and ILS due to the wide concentration ranges and the limited number of samples in the MLS. After Welch's ANOVAs, Games-Howell post-hoc tests were applied to verify where there were significant differences. Comparisons of CH_4 concentrations above and below the pycnocline were made using t-tests assuming unequal variances. All statistical results (F-values, degrees of freedom, n-values, p-values and adjusted p-values) are reported in the Supplementary Tables S1-S5.

Sequencing data indicated three microbial types of hopanoid producers (Fig.S1&S2) and no evidence for anammox bacteria. Aerobic methanotrophs and heterotrophs were most common and therefore used as the two endmembers for hopanoid source apportionment. The hopanoid source apportionment was calculated through a Bayesian stable carbon isotope mixing model using two endmembers (MOB & heterotrophic bacteria) applied with "simmr" in RStudio (Parnell et al., 2013). Due to a larger isotope fractionation in MOB-I hopanoid synthesis compared to MOB-II (Jahnke et al., 1999), the relative contribution of the different AeOM pathways was estimated using the relative abundance of MOB-I versus MOB-II within each sample (Eq.2). Since 16S-rRNA does not indicate the relative activity of these microbes, this approach is a semi-quantitative estimation of CH_4-related hopanoid production. The associated isotope endmembers and isotope fractionation during hopanoid biosynthesis are displayed in Supplementary Tables S6 & S7 and further described in Eqs. 2-4, where f_{MOB-I} and f_{MOB-II} are the fractions of MOB based on the relative abundance of 16S-rRNA. The $\Delta\delta^{13}C_{MOB-I/II}$ and $\Delta\delta^{13}C_{DOC}$ describe the isotope fractionation from CH_4 to hopanoid and dissolved OC to hopanoid, respectively.

$$\delta^{13}C_{MOB} = f_{MOB-I} * (\delta^{13}C_{CH4} + \Delta\delta^{13}C_{MOB-I}) + f_{MOB-II} * (\delta^{13}C_{CH4} + \Delta\delta^{13}C_{MOB-II}) \qquad (2)$$

$$\delta^{13}C_{Heterotroph} = \delta^{13}C_{DOC} + \Delta\delta^{13}C_{DOC} \qquad (3)$$

$$CH_{4\text{-derived hopanoids (\%)}} = \frac{(\delta^{13}C_{hopanoid} - \delta^{13}C_{Heterotroph})}{(\delta^{13}C_{MOB} - \delta^{13}C_{Heterotroph})} \times 100 \tag{4}$$

3 Results

3.1 Large-scale spatial patterns of dissolved CH₄ concentrations

275   The dissolved CH_4 concentrations in the Laptev Sea were high compared to the atmospheric equilibrium at ~4 nM. The sub-pycnocline CH_4 concentrations for the 26 studied stations varied widely between 8 and 11 850 nM (median = 278 (IQR = 88-966) nM), with the highest concentrations at station 47 in the Outer Laptev Sea hotspot region (OLS; Fig.2). The sub-pycnocline CH_4 concentrations were significantly different between all regions (Table S1). The CH_4 concentrations in the OLS (defined as latitudes ≥ 76.1° N & longitudes 125-131°E) were significantly higher compared to the Inner and Mid Laptev Sea

280   (ILS/MLS; defined as latitudes <73.9 °N & 73.9-76.1°N & longitudes ~130°E, respectively; Table S1). In all regions, dissolved CH_4 was significantly lower in the surface water compared to below the pycnocline (Table S2). Additionally, surface water CH_4 was significantly higher in the ILS hotspot region (Table S3) compared to the MLS and OLS (Table S3).
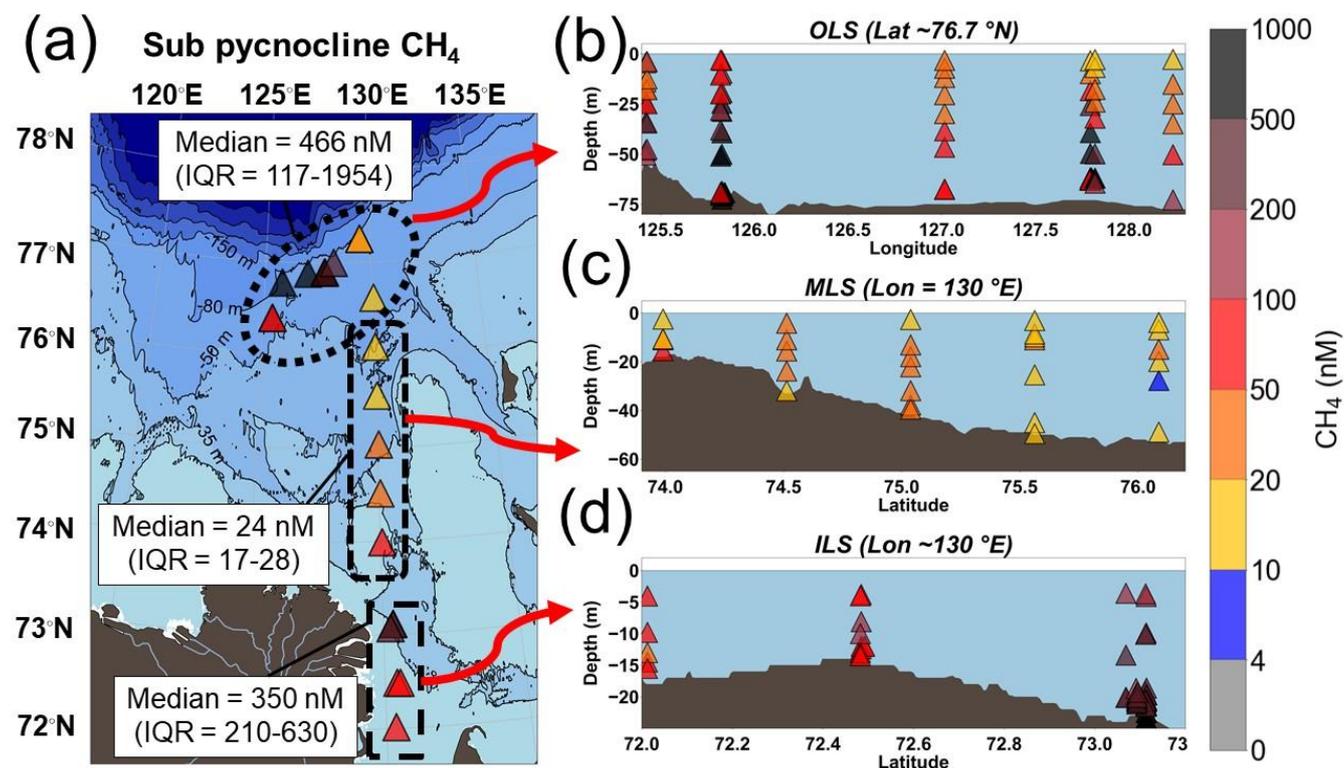
Figure 2. Dissolved CH_4 concentrations (nM). (a) Average CH_4 concentrations below the pycnocline. (b) The outer Laptev Sea hotspot region (OLS). (c) Mid-Outer Laptev Sea transect (MLS). (d) The inner Laptev Sea hotspot region (ILS). The bathymetry was plotted using IBCAO version 5.0 (Jakobsson et al., 2024).

3.2 Organic geochemistry

3.2.1 Bulk organic carbon

The total Organic Carbon (OC) content displayed strong variability across the Laptev Sea. The total OC varied between 0.2 and 2.3 % (mean±standard deviation; 1.0±0.5%, n=25), with the lowest concentrations observed in the the OLS (0.9±0.4, n=14), and higher concentrations in the MLS (1.0±0.5, n=5) and ILS (1.3±0.8, n=6). The $\delta^{13}C$-OC ranged from -26.8 to -23.3 ‰ (-24.7±1.0 ‰, n=25), with the highest values in the OLS (-23.9±0.4, n=14) and slightly lower values in the MLS (-25.0±0.7, n=5) and the ILS (-26.1±0.5, n=6).

3.2.2 Hopanoid lipid concentrations and spatial distribution patterns

Hopanoids were present at detectable levels across all surface sediments. The sum of C_{30}-hopenes ($\sum C_{30}$-hopenes; diploptene, hop-17(21)-ene and neohop-13(18)-ene) displayed a large range of concentrations across the Laptev Sea (mean±standard deviation; 27±19 µg gOC^{-1}; n=25). The highest concentrations were found in the OLS (35±20 µg gOC^{-1}; n=15; Fig.5). Relatively high $\sum C_{30}$-hopenes concentrations were also present in the ILS, with no significant difference compared to the OLS (18±11 µg gOC^{-1}; n=6; Fig.5; Supplementary Table 4). In contrast, the concentrations of $\sum C_{30}$-hopenes were significantly lower in the MLS (10±4 µg gOC^{-1}; n=4; Fig.5) compared to the OLS, but did not show significantly different concentrations compared to the ILS (Supplementary Table 4). The large standard deviation of hopanoid concentrations in the OLS and ILS is likely related to the presence of main "hotspot" stations, causing a log-normal distribution of the data. On average, diploptene (hop-22(29)-ene) comprised the majority of C_{30}-hopenes (68%), with a lower abundance of its diagenetic products (hop-17(21)-ene and neohop-13(18)-ene; 19 & 13%). While diploptene dominated the C_{30}-hopene abundance across all regions, it comprised a larger part of the C_{30}-hopenes in the ILS (74%) compared to the MLS and OLS (52% & 69%, respectively). In the MLS in particular, hop-17(21)-ene and neohop-13(18)-ene constituted a larger part of the $\sum C_{30}$-hopenes (31 % & 18 %).

3.3.3 Hopanoid isotope composition and spatial distribution patterns

The compound-specific isotope composition of $\delta^{13}C$-C_{30}-hopenes (diploptene, hop-17(21)-ene and neohop-13(18)-ene) in the Laptev Sea was remarkably depleted compared to the bulk OC. The $\delta^{13}C$-C_{30}-hopenes were on average -47.8±7.2 ‰ (mean±standard deviation; n=23; Fig.5). The $\delta^{13}C$-C_{30}-hopenes were lowest in the OLS, with a mean±standard deviation of -52.9±4.3 ‰ across the region (Fig.5). Hopanoids in MLS and ILS exhibited depleted but relative to the OLS more enriched $\delta^{13}C$-C_{30}-hopenes (-42.0±1.9 ‰ & -39.4±3.0‰; Fig.5). No significant differences were observed between the two regions (Table S5), yet both were much more depleted than their regional $\delta^{13}C$-OC.

Amongst the C_{30}-hopanoids, $\delta^{13}C$-diploptene and diplopterol displayed the lowest values in the OLS (-59.5 & -61.0 ‰; Fig.3). Hop-17(21)-ene and neohop-13(18)-ene likewise demonstrated low $\delta^{13}C$, yet neohop-13(18)-ene was more enriched in ^{13}C in the OLS (Fig. 3). However, in the MLS/ILS diploptene and diplopterol in particular were more enriched in $\delta^{13}C$, up to a maximum of -34.1 & -29.0 ‰, respectively (Fig.3). On the contrary, $\delta^{13}C$ of hop-17(21)-ene exhibited lower values compared to diploptene in the ILS (-41.9±4.6 ‰ & -37.6±2.2 ‰; Fig.3). While diplopterol was also present in the ILS samples, coelution with other molecules hindered accurate concentration and isotope measurements due to interferences. Hence, $\delta^{13}C$-diplopterol was not quantified in the ILS. In summary, $\delta^{13}C$-C_{30}-hopanoids were generally low across the Laptev Sea, especially in the OLS. However, in the ILS, hop-17(21)-ene was more depleted in comparison to other hopanoids (Fig.3).
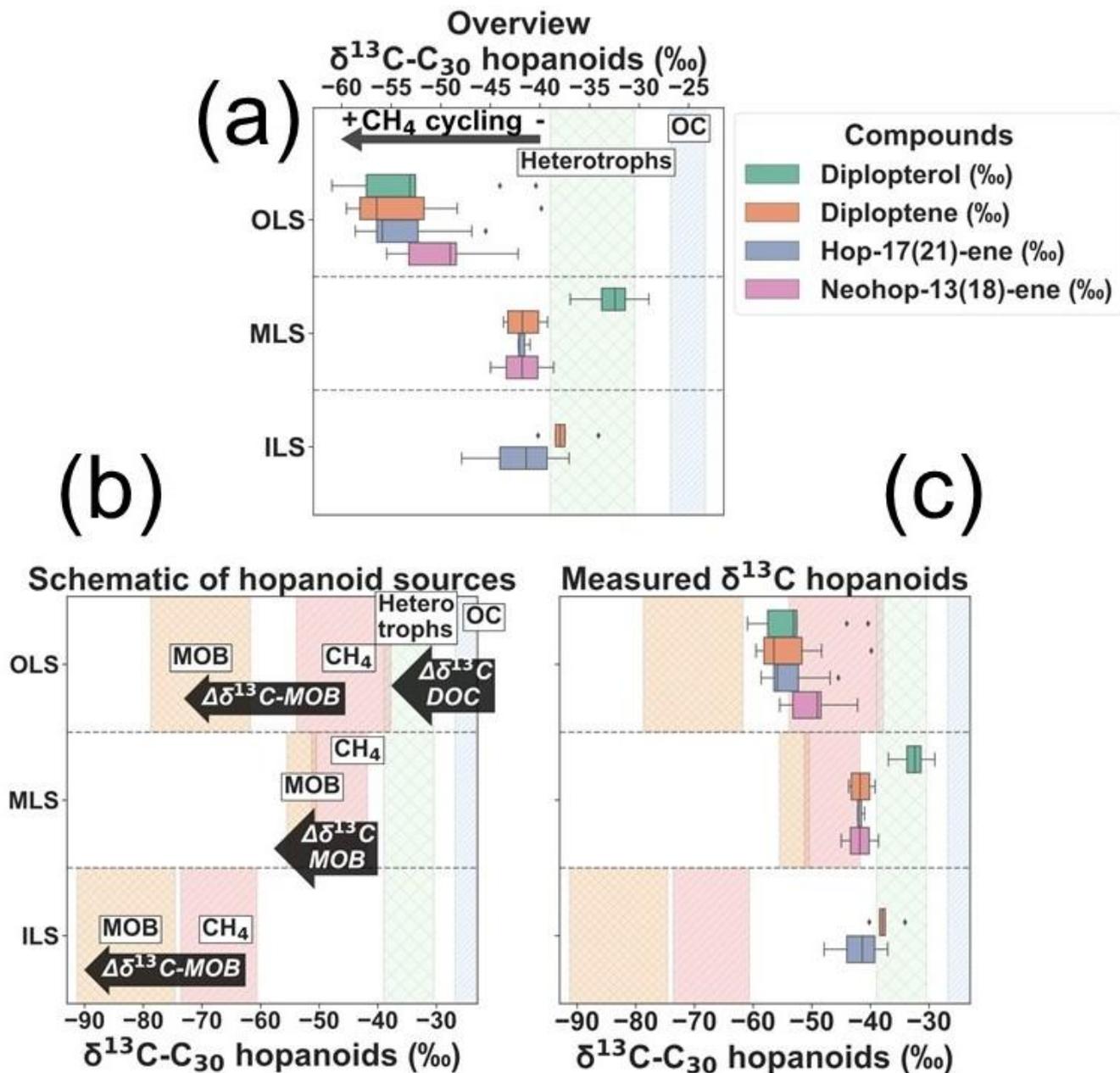
325

12

Figure 3. (a) Overview of the measured $\delta^{13}C$ of individual C_{30} hopanoids across each region. The shaded green zone indicates the range of $\delta^{13}C$-heterotrophic hopanoids by production from DOC after isotope fractionation during hopanoid synthesis (Supplementary Tables S6 & S7; Salvado et al., 2016; Schwartz et al., 2023). The light blue indicates the measured $\delta^{13}C$-OC in this study. (b) Schematic of $\delta^{13}C$ of carbon substrates used for hopanoid production and the associated isotope fractionation ($\Delta\delta^{13}C$; Supplementary Tables S6 & S7; Jahnke et al., 1999; Salvadó et al., 2016; Steinbach et al., 2021; Schwartz et al., 2023; Brussee et al., 2026). Semi-quantitative estimations of the Methane Oxidizing Bacteria (MOB; orange) in each region are the $\delta^{13}C$-hopanoid endmembers, where the isotope fractionation of MOB-I and II, respectively, was weighted against the relative fraction of MOB (Eq. 2). The pink displays the $\delta^{13}C$-CH$_4$ in each investigated region (Supplementary Table S6). (c) Measured $\delta^{13}C$-C_{30} hopanoids compared against the hopanoid and carbon source endmembers in each region.

13

3.3 Bacterial consortia of hopanoid producers

Aerobic methanotrophs, here referred to as Methane Oxidizing Bacteria (MOB), were present in 9 out of the 11 sediment samples probed for 16S-rRNA. Both type I (*Gammaproteobacteria*; MOB-I) and type II (*Alphaproteobacteria*; MOB-II, Fig.4; Fig.S1) MOB were detected in those 9 samples. Type I MOB constituted the majority of the MOB in the OLS compared to MOB-II (mean±standard deviation;1.2±1.8 % of all sequences, n =5; 0.10±0.08, n=3; Fig.4). Specifically, the highest relative abundance of MOB-I was present at station 47 (4.3 %: Fig.3). While the relative abundances of MOB were overall low in the MLS, MOB-II were more abundant (0.04±0.01 n = 2 & 0.01±0.01, n=2; Fig.4). On the other hand, in the ILS MOB I and II were of similar relative abundances (0.18±0.15 %, n =2 & 0.17±0.15 %, n=3), yet almost a factor ten lower than in the OLS. The most common MOB-I were of the order *Methylococcales*, specifically of the genera *Methyloprofundus* and *Marine methylotrophic group 2* (Fig.S1). Other common type I MOB in the Laptev Sea were *pLW-20, Milano-WF1B-03*, *Milano-WF1B-42* and *pItb-vmat-59* (Fig.S1). *Crenothrix* was only detected in the ILS (Fig. 4; Fig. S1) and *IheB2-23* and *Cycloclasticus* only at the OLS stations (Fig.S1). Candidates of Type II MOB were of the family *Methyloligellaceae*¸ with one identified genus known to produce hopanoids (*Methyloceanibacter*). However, it should be recognized that not all *Methyloligellaceae* are necessarily methanotrophs. In addition to MOB, heterotrophic and autotrophic hopanoid producers were present in the Laptev Sea, particularly in the ILS (Fig.S2). Taken together, MOB-I constituted the largest part of the bacterial hopanoid producers in the OLS, with almost ten times higher relative abundance compared to the MLS/ILS. Hopanoid producers in the ILS/MLS were a mix of MOB-I/II and non-methanotrophic hopanoid producers, primarily heterotrophic bacteria (Fig.4).
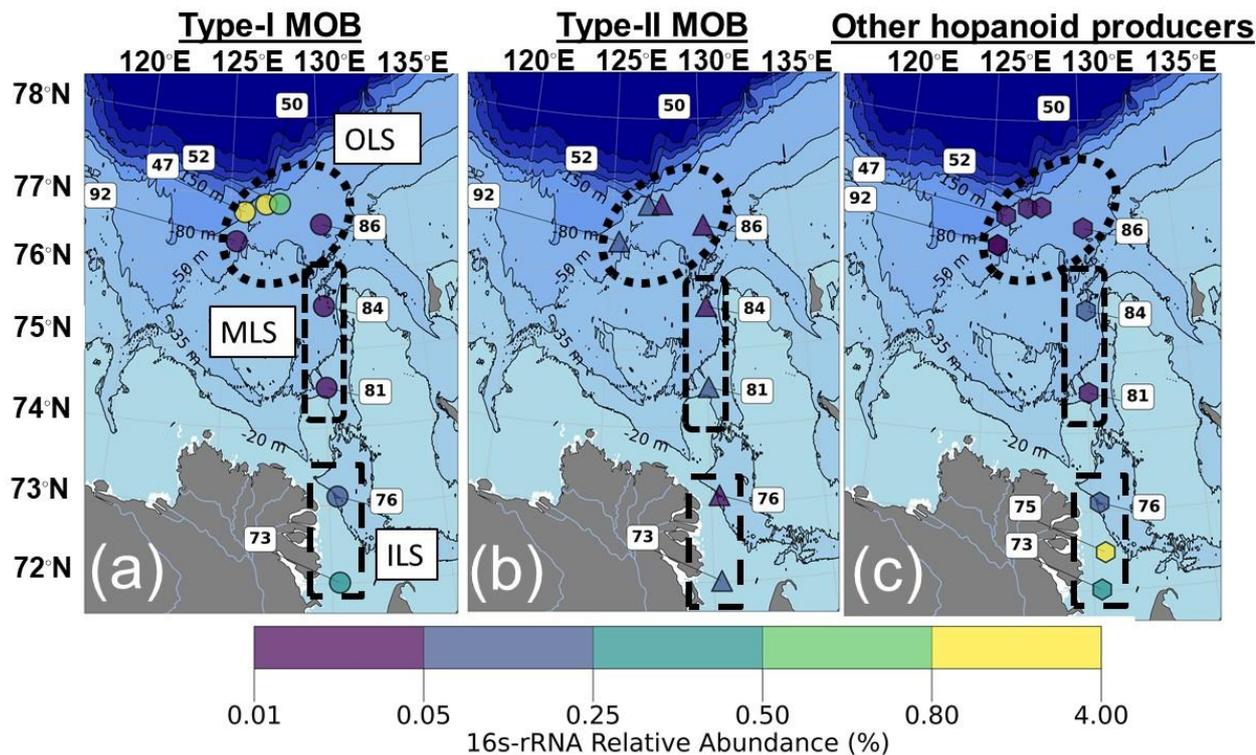
Figure 4. Relative abundance of hopanoid producers in the surface sediments (%), based on 16S-rRNA. (a) Type I MOB. (b) Type II MOB. (c) Other hopanoid producers. The bathymetry was plotted using IBCAO version 5.0 (Jakobsson et al., 2024).

4 Discussion

4.1 Indications of widespread enhanced methane cycling across the Laptev Sea displayed by lipid biomarkers

Depleted δ^{13}C-C$_{30}$ hopanoids in surface sediments indicate large-scale enhanced CH$_4$ cycling across the Laptev Sea. As the Laptev Sea water and surface sediments are well oxygenated (Stepanova et al., 2017; Brüchert et al., 2018; Maciute et al., 2025), the CH$_4$ signal in hopanoids is most likely related to aerobic processes. The Laptev Sea is frequently ventilated through storms, resulting in a wide variety of dissolved CH$_4$ concentrations dependent on the time of sampling relative to storm ventilation of the water column CH$_4$ (e.g., Shakhova et al., 2014). In contrast, the CH$_4$ signal from δ^{13}C-C$_{30}$ hopanoids accumulated in sediments indicates a CH$_4$ signal averaged over several years. Thus, δ^{13}C-C$_{30}$ hopanoids provide means to assess long-term CH$_4$ cycling patterns compared to the ephemeral dissolved CH$_4$ concentrations in the Laptev Sea. Hence, the δ^{13}C-C$_{30}$ hopanoids help to unearth CH$_4$ dynamics in a region that is hard to access and thereby void of time-series monitoring of CH$_4$. The proxy-derived CH$_4$ signal in the isotopes of these hopanoids also corroborates previous suggestions of the Laptev Sea as a region of widespread CH$_4$ cycling in the water column (e.g., Semiletov, 1999; Shakhova et al., 2010, 2013, 2014; Steinbach et al., 2021).

15
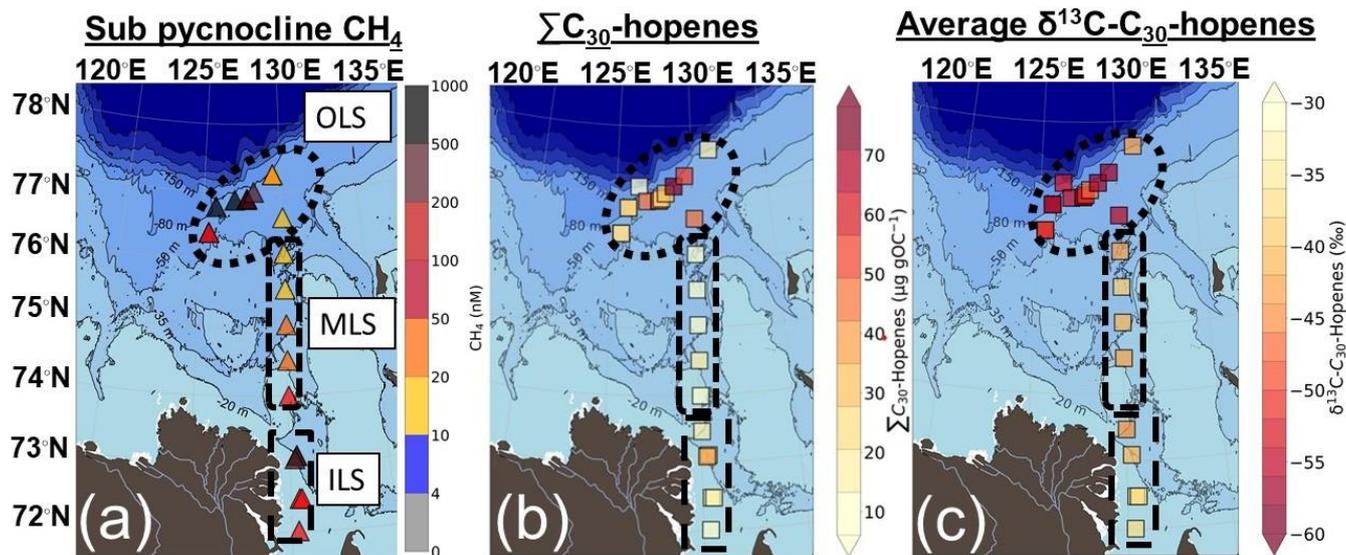
Figure 5. (a) Sub pycnocline CH_4 concentrations, (b) the total concentration of C_{30} hopenes (diploptene, hop-17(21)-ene & neohop-13(18)-ene; µg gOC^{-1}) and (c) the average $\delta^{13}C$-C_{30} hopenes (‰) in Laptev Sea surface sediments. The bathymetry was plotted using IBCAO version 5.0 (Jakobsson et al., 2024).

4.2 Spatial variations of methane concentrations and hopanoid-isotope patterns

4.2.1 Intensive CH_4 cycling in the Outer Laptev Sea hotspot region

The high abundance of very depleted $\delta^{13}C$-C_{30} hopanoids in the OLS highlights ubiquitous enhanced CH_4 cycling through AeOM across this region (Fig.5). High concentrations of C_{30} hopenes in the OLS hotspot region are broadly consistent with previous observations of diploptene from surface sediments sampled in this area in 2011 and 2016 (Grinko et al., 2020, 2025). Beyond earlier studies, our findings of depleted $\delta^{13}C$-C_{30} hopanoids in this region confirm a methanotrophic source of the hopanoids. The presence of very low $\delta^{13}C$-C_{30} hopanoids in the OLS is a strong indication of MOB-I, which is further corroborated by 16S-rRNA (Fig.4 &5). Indeed, the application of a stable isotope mixing model (Eq.4) suggests that 59±4 % of hopanoids in the OLS are related to MOB-I and II. As the mixing model is weighted against the abundance of MOB-I and II and not their respective activity, these results should be regarded as semi-quantitative. Nonetheless, it supports the hypothesis of CH_4 incorporation in hopanoids. Additionally, diplopterol is slightly more depleted in ^{13}C in the OLS compared to other C_{30} hopanoids; this might reflect increased depletion in ^{13}C of hopanoids for each step in the biosynthetic pathway (i.e., ^{13}C isotope depletion from squalene to diploptene, to diplopterol; Summons et al., 1994). In short, very low values of $\delta^{13}C$-C_{30} hopanoids together with high CH_4 concentrations and a high relative abundance of MOB-I indicate the OLS as a region of extensive CH_4 emissions and associated AeOM (Fig.2b&5).

16

4.2.2 AeOM-biomarkers tracing methane cycling in the Mid-Outer Laptev Sea transect

In the MLS, lower yet readily detectable C_{30} hopene concentrations suggest less MOB biomass present in this region.
390   Nonetheless, the depleted $\delta^{13}C$-C_{30} hopenes signals and presence of MOB in the MLS regime indicate hopanoids tracing CH_4 cycling (Fig. 4 & 5), with the source apportionment indicating that MOB contributed to 55±15 % of the hopanoid production. In situ hopanoid production in the MLS region or surface water transport of hopanoids from the ILS hotspot are possible causes. Given that CH_4 concentrations are higher in the sub-pycnocline waters of the MLS than in the surface water, where transport from the ILS would be centered and that a larger fraction of hopanoids comes from MOB compared to in the ILS, it
395   seems likely that most hopanoids in the MLS are locally produced. Prior assessments have considered the MLS as a region of continuous subsea permafrost and comparatively low CH_4 concentrations (Shakhova et al., 2010; Bukhanov et al., 2023). In contrast, here we show a proxy-derived record of CH_4 in a region that was previously conceived as being of low CH_4 cycling. However, additional modern calibrations of these hopanoid proxy tools in regions with lower CH_4 concentrations are necessary to confirm whether this indicates an onset of enhanced CH_4 cycling, or if it is regarded as a "background signal" of CH_4-related
400   hopanoids in marine systems. Taken together, we display a record of biomarker proxy-derived CH_4 in the MLS, most likely dominated by a more diffuse regional CH_4 source in the MLS. The presence of low $\delta^{13}C$-C_{30} hopenes across the Laptev Sea indicates the potential to trace proxy-derived CH_4 in all investigated regions and displays important factors to consider when interpreting such biomarker records.

4.2.3 Varying hopanoid sources in the Inner Laptev Sea hotspot region

405   High concentrations of CH_4, depleted $\delta^{13}C$-C_{30} hopenes values and the presence of MOB highlight the possibility of tracing CH_4 cycling also in the ILS. However, while concentrations of C_{30} hopenes were relatively high and not significantly different from those in the OLS, the $\delta^{13}C$-C_{30} hopenes in the ILS are less depleted. This can be interpreted in different ways, but is likely a combination of three mechanisms: (1) the relative contribution from MOB-I and II, (2) isotopic dilution from non-methanotrophic sources and (3) lower activity of AeOM in the ILS compared to the OLS. In contrast to the OLS, a higher
410   relative abundance of MOB-II is present in relation to MOB-I in the ILS. Type II MOB can produce hopanoids more enriched in ^{13}C compared to MOB-I due to their ability to also assimilate CO_2 into biomass (Jahnke et al., 1999). *Methyloceanibacter* constituted the only genus of MOB-II in the ILS (Fig. S1) and have to our knowledge only been isolated from marine systems (Takeuchi et al., 2014, 2019; Vekeman et al., 2016). Thus, the MOB-II present in our study is likely an in situ signal of AeOM rather than of coastal influence as was found in the Kara Sea/Yenisei River (de Jonge et al., 2016), despite MOB-II generally
415   dominating terrestrial ecosystems (Hanson & Hanson, 1996; Inglis et al., 2019). Noteworthy, $\delta^{13}C$-C_{30} hopenes values ~-40 ‰ has in contemporary peatland settings been interpreted as a strong indication of enhanced CH_4 cycling related to MOB-II (Inglis et al., 2019). In fact, even $\delta^{13}C$-diploptene as high as -35 ‰ has been interpreted as an indication of AeOM in the Cariaco Trench (Freeman et al., 1994), due to co-occurring autotrophic biomarkers with a $\delta^{13}C$ composition of >4 ‰ higher than diploptene (Freeman et al., 1994). Therefore, the less depleted $\delta^{13}C$-C_{30} hopenes, yet in similar concentrations to the OLS,

420 can be an indication of MOB-II and shows that a proxy-derived CH_4 signal in coastal regions needs thorough system knowledge
to depict the source.

The higher $\delta^{13}C$-C_{30} hopenes in the ILS compared to the OLS can also be explained by a dilution of hopanoid production from
non-methanotrophic bacteria. Hopanoids (e.g., diploptene, hop-17(21)-ene) are directly synthesized or produced as
425 degradation products of bacteriohopanepolyols (BHPs; Rohmer et al., 1980; Mackenzie et al., 1981). A mixture of hopanoid
sources is to be expected, as ~10 % percent of bacteria can synthesize hopanoids (Ourisson et al., 1979; Fischer et al., 2005;
Racolta et al., 2012; Belin et al., 2018). Relatively high concentrations of bacteriohopanetetrol (BHT) have previously been
found in the ILS and have been attributed to terrestrial sources (Bischoff et al., 2016). This study thereby indicates that a
dilution from non-methanotrophic terrestrial sources may contribute to the higher $\delta^{13}C$-C_{30} hopenes, due to the vicinity of the
430 Lena River delta and higher relative abundance of non-methanotrophic hopanoid producers compared to MOB. This is further
strengthened by $\delta^{13}C$-OC around ~26‰, indicating a larger terrestrial loading to the sediments of the ILS. Hopanoid source
apportionment displayed that 77±7 % of hopanoids in the ILS are related to non-methanotrophic hopanoid synthesis and 16S-
rRNA data indicate that the "other hopanoid producers" are partly of terrestrial origin (Fig.4; Fig.S2). Consequently, the
presence of hopenes more enriched in ^{13}C is also an indication of an additional contribution from non-methanotrophic hopanoid
435 sources, rather than reflecting lower CH_4 cycling in this region. It should also be noted that the high CH_4 concentrations in the
ILS originate from an old biogenic source in the coastal region (Sapart et al., 2017) and not riverine input of CH_4 (Shakhova
& Semiletov, 2007; Shakhova et al., 2010, 2014, 2017).

Despite high CH_4 concentrations in the ILS, higher $\delta^{13}C$-C_{30} hopenes compared to the OLS hotspot region could alternatively
440 also indicate less active AeOM. Incubation experiments of ILS surface sediments and water show the possibility of AeOM
(Bussmann et al., 2017, 2021; Tikhonova et al., 2021), yet at lower rates compared to the OLS (Tikhonova et al., 2021). Taken
all together, the relative enrichment of $\delta^{13}C$-hopenes in the ILS compared to the OLS hotspot is likely a combination of: (1) a
higher relative input of hopanoids from MOB-II, (2) non-methanotrophic bacteria produced in situ and in terrestrial settings
and (3) lower activity of AeOM compared to the OLS. Nonetheless, the depleted $\delta^{13}C$-hop-17(21)-ene does indicate the
445 presence of AeOM and thereby traces CH_4 cycling (Fig.3).

4.3 Large-scale implications for Laptev Sea CH_4 cycling

Since the discovery two decades ago, the Laptev Sea CH_4 dynamics and sources have been increasing. It has been suggested
that gas-hydrate-bearing sediments in the region store vast amounts of CH_4 (Soloviev, 2000), functioning as a possible CH_4
source upon destabilization (e.g., Shakhova et al., 2010, 2011). Thawing subsea permafrost has also been suggested as a source
450 of CH_4 in the ILS (Shakhova et al., 2014; Sapart et al., 2017) and to serve as a conduit for leakage of deep thermogenic CH_4
gas reservoirs in the OLS (Steinbach et al., 2021). Our biomarkers of AeOM across the Laptev Sea indicate the presence of a
microbial sink, but the high CH_4 concentrations question its efficiency. Historically, a large focus has been given to the ILS

and OLS regions with detected CH$_4$ ebullition (e.g., Shakhova et al., 2010, 2014; Sapart et al., 2017; Steinbach et al., 2021), but few investigations have paid attention to the MLS as the observations have reported lower CH$_4$ concentrations in that region, yet still elevated relative to atmospheric partial pressures. Thus, our indications of enhanced CH$_4$ cycling in the MLS stimulate a few questions. (1) Why has subsea permafrost-related CH$_4$ release only been observed in the ILS/OLS? (2) Is the CH$_4$ activity in the MLS linked to ILS CH$_4$ cycling, or is there a large-scale diffuse source across the MLS?

Many challenges still exist regarding our understanding of the state of current subsea permafrost and associated CH$_4$ releases. In situ bottom sediment temperatures point towards thawing permafrost in the ILS/OLS CH$_4$ hotspot regions (Chuvillin et al., 2022; Bukhanov et al., 2023). However, the state of the subsea permafrost and consequent CH$_4$ releases from these two regions are likely caused by different mechanisms. Inundation of the OLS and accompanied heat exposure from both Atlantic water and underlying fault zones transporting geothermal heat have likely contributed to its warming thermal state (Chuvillin et al., 2022). Indeed, areas of warmer sediment temperatures in the OLS are coinciding with CH$_4$ seepages and underlying fault zones (Baranov et al., 2020; Chuvillin et al., 2022). In the ILS, heat flux from the Lena River is proposed to be the main mechanism thawing subsea permafrost, but thawing is also likely induced by geothermal heat through the Ust' Lenskii Rift (Chuvillin et al., 2022; Bukhanov et al., 2023). Additionally, the bottom water from the Lena River plume has increased by ~1°C between 1999-2012 (Shakhova et al., 2014) during which time subsea permafrost has rapidly thawed (Shakhova et al., 2017). Thus, the state of subsea permafrost and lower CH$_4$ cycling in the MLS can be related to the mechanisms regulating the thermal state of subsea permafrost (i.e., heat flux from geothermal or riverine sources).

The surface water CH$_4$ concentrations in the MLS are lower than in the ILS and OLS, yet they exceed the atmospheric equilibrium (4 nM) by ~4.6 times (median = 18.6 nM). However, the source of CH$_4$ in the MLS is not fully clear. Assuming that a regional CH$_4$ source is present in the MLS, further investigations are necessary, especially if it is related to the subsea permafrost thaw-state. In situ bottom sediment temperatures indicate that the MLS is on the border of discontinuous/continuous subsea permafrost (Chuvillin et al., 2022; Bukhanov et al., 2023) and thus possibly on the "thaw-front", which could be an indication of the thaw-state regulating the CH$_4$ emissions from the MLS. If a regional-MLS source of CH$_4$ is present in this region, the source of these CH$_4$ emissions and the associated AeOM needs to be further investigated. Taken together, there may be geospatial thaw fronts of the subsea permafrost from the OLS moving inwards and from the ILS moving outwards, thus both over time leading to a shrinking MLS transition zone and growing coverage of the extensive areas with accompanying CH$_4$ releases.

5 Conclusions

This study demonstrates that δ^{13}C-C$_{30}$ hopanoids can be used as time-integrated proxies to deduce geospatial patterns of CH$_4$ cycling from marine sediments. A clear signal of CH$_4$ being incorporated into hopanoids is shown throughout the wide outer

485 Laptev Sea hotspot region, indicating the possibility to also investigate time trends of enhanced CH_4 cycling from this region in chronologically-constrained sediment cores. Additionally, a signal of enhanced CH_4 cycling is discovered in the Mid-Outer Laptev Sea transect (MLS), previously thought to be a region of comparatively low CH_4 cycling. The MLS signal could be derived from the Inner Laptev Sea hotspot (ILS), yet, more likely, from a diffuse source in the MLS itself. In the ILS, high CH_4 concentrations were less well reflected in the molecular fossils, indicating AeOM, yet still indicative of CH_4. This is

490 attributed to a higher relative abundance of MOB-II that utilize both CH_4 and CO_2 for hopanoid production, isotopic mixing with non-methanotrophic bacteria, partly of terrestrial origin, producing hopanoids, but also less active AeOM in the ILS hotspot. This indicates that complementary evidence to $\delta^{13}C$-C_{30} hopanoids and thorough system knowledge is necessary in coastal settings in the vicinity of large rivers. However, low AeOM in a region of high CH_4 concentrations, such as the ILS, could have consequences for the amount of CH_4 emitted to the atmosphere. To the best of our knowledge, this is the first

495 modern calibration of $\delta^{13}C$-hopanoids over an extensive marine setting, facilitating improved interpretations of hopanoid sources in contemporary and past climates. Furthermore, this study provides a large-scale geospatial picture of Laptev Sea CH_4 cycling, with considerations for future studies of CH_4 cycling in the circum-Arctic shelf regions.

Data availability

The supplementary information (pdf-file) contains the composition of hopanoid producers, results from statistical analyses,

500 chromatograms, and mass spectra of biomarkers. The supplementary data can be accessed through the Bolin Centre Database (https://doi.org/10.17043/eriksson-2026-biomarker-1) and the code to run the stable isotope mixing model through "simmR" is provided in "Supplementary Code".

Acknowledgements

Financial support

References

Apprill, A., Mcnally, S., Parsons, R., and Weber, L.: Minor revision to V4 region SSU rRNA 806R gene primer greatly increases detection of SAR11 bacterioplankton, Aquatic Microbial Ecology, 75, 129–137, https://doi.org/10.3354/ame01753, 2015.

Baranov, B., Galkin, & S., Vedenin, & A., Dozorova, & K., Gebruk, & A., and Flint, & M.: Methane seeps on the outer shelf of the Laptev Sea: characteristic features, structural control, and benthic fauna, https://doi.org/10.1007/s00367-020-00655-7/Published, n.d.

Belin, B. J., Busset, N., Giraud, E., Molinaro, A., Silipo, A., and Newman, Di. K.: Hopanoid lipids: From membranes to plant-bacteria interactions, https://doi.org/10.1038/nrmicro.2017.173, 1 May 2018.

Birgel, D. and Peckmann, J.: Aerobic methanotrophy at ancient marine methane seeps: A synthesis, Org Geochem, 39, 1659–1667, https://doi.org/10.1016/j.orggeochem.2008.01.023, 2008.

Bischoff, J., Sparkes, R. B., Selver, A. D., Spencer, R. G. M., Gustafsson, Ö., Semiletov, I. P., Dudarev, O. V., Wagner, D., Rivkina, E., Van Dongen, B. E., and Talbot, H. M.: Source, transport and fate of soil organic matter inferred from microbial

biomarker lipids on the East Siberian Arctic Shelf, Biogeosciences, 13, 4899–4914, https://doi.org/10.5194/bg-13-4899-2016, 2016.

Blumenberg, M., Naafs, B. D. A., Lückge, A., Lauretano, V., Schefuß, E., Galloway, J. M., Scheeder, G., and Reinhardt, L.: Biomarker Reconstruction of a High-Latitude Late Paleocene to Early Eocene Coal Swamp Environment Across the PETM and ETM-2 (Ellesmere Island, Arctic Canada), Paleoceanogr Paleoclimatol, 39, https://doi.org/10.1029/2023PA004712, 2024.

Brussee, M., Holmstrand, H., Wild, B., Kosmach, D., Chernykh, D., Shakhova, N., Kurilenko, A., Semiletov, I., and Gustafsson, Ö.: Triple-isotopic analyses pinpoint microbial methane release from subsea permafrost in the inner Laptev Sea, Commun Earth Environ, https://doi.org/10.1038/s43247-026-03222-7, 2026.

Bukhanov, B., Chuvilin, E., Zhmaev, M., Shakhova, N., Spivak, E., Dudarev, O., Osadchiev, A., Spasennykh, M., and Semiletov, I.: In situ bottom sediment temperatures in the Siberian arctic seas: Current state of subsea permafrost in the kara sea vs laptev and east Siberian seas, Mar Pet Geol, 157, https://doi.org/10.1016/j.marpetgeo.2023.106467, 2023.

Bussmann, I., Hackbusch, S., Schaal, P., and Wichels, A.: Methane distribution and oxidation around the Lena Delta in summer 2013, Biogeosciences, 14, 4985–5002, https://doi.org/10.5194/bg-14-4985-2017, 2017.

Bussmann, I., Fedorova, I., Juhls, B., Paul Overduin, P., and Winkel, M.: Methane dynamics in three different Siberian water bodies under winter and summer conditions, Biogeosciences, 18, 2047–2061, https://doi.org/10.5194/bg-18-2047-2021, 2021.

Bröder, L., Tesi, T., Andersson, A., Semiletov, I., and Gustafsson, Ö.: Bounding cross-shelf transport time and degradation in Siberian-Arctic land-ocean carbon transfer, Nat Commun, 9, https://doi.org/10.1038/s41467-018-03192-1, 2018.

Brüchert, V., Bröder, L., Sawicka, J. E., Tesi, T., Joye, S. P., Sun, X., Semiletov, I. P., and Samarkin, V. A.: Carbon mineralization in Laptev and East Siberian Sea shelf and slope sediment, Biogeosciences, 15, 471–490, https://doi.org/10.5194/bg-15-471-2018, 2018.

Callahan, B. J., McMurdie, P. J., Rosen, M. J., Han, A. W., Johnson, A. J. A., and Holmes, S. P.: DADA2: High-resolution sample inference from Illumina amplicon data, Nat Methods, 13, 581–583, https://doi.org/10.1038/nmeth.3869, 2016.

Chernykh, D., Shakhova, N., Yusupov, V., Gershelis, E., Morgunov, B., and Semiletov, I.: First Calibrated Methane Bubble Wintertime Observations in the Siberian Arctic Seas: Selected Results from the Fast Ice, Geosciences (Switzerland), 13, https://doi.org/10.3390/geosciences13080228, 2023.

Chuvilin, E., Bukhanov, B., Yurchenko, A., Davletshina, D., Shakhova, N., Spivak, E., Rusakov, V., Dudarev, O., Khaustova, N., Tikhonova, A., Gustafsson, O., Tesi, T., Martens, J., Jakobsson, M., Spasennykh, M., and Semiletov, I.: In-situ temperatures and thermal properties of the East Siberian Arctic shelf sediments: Key input for understanding the dynamics of subsea permafrost, Mar Pet Geol, 138, https://doi.org/10.1016/j.marpetgeo.2022.105550, 2022.

Damsté, J. S. S., Rijpstra, W. I. C., Dedysh, S. N., Foesel, B. U., and Villanueva, L.: Pheno- and genotyping of hopanoid production in Acidobacteria, Front Microbiol, 8, https://doi.org/10.3389/fmicb.2017.00968, 2017.

Davies, K. L., Pancost, R. D., Edwards, M. E., Walter Anthony, K. M., Langdon, P. G., and Torres, L. C.: Diploptene δ13C values from contemporary thermokarst lake sediments show complex spatial variation, Biogeosciences, 13, 2611–2621, https://doi.org/10.5194/bg-13-2611-2016, 2016.

De Jonge, C., Talbot, H. M., Bischoff, J., Stadnitskaia, A., Cherkashov, G., and Sinninghe Damsté, J. S.: Bacteriohopanepolyol distribution in Yenisei River and Kara Sea suspended particulate matter and sediments traces terrigenous organic matter input, Geochim Cosmochim Acta, 174, 85–101, https://doi.org/10.1016/j.gca.2015.11.008, 2016.

Elvert, M. and Niemann, H.: Occurrence of unusual steroids and hopanoids derived from aerobic methanotrophs at an active marine mud volcano, Org Geochem, 39, 167–177, https://doi.org/10.1016/j.orggeochem.2007.11.006, 2008.

Fischer, W.W., Summons, R.E., and Pearson, A.: Targeted genomic detection of biosynthetic pathways: anaerobic production of hopanoid biomarkers by a common sedimentary microbe, Geobiology, 3, 33-40, https://doi.org/10.1111/j.1472-4669.2005.00041.x, 2005.

Freeman, K. H., Wakeham, S. G., and Hayes, J. M.: Predictive isotopic biogeochemistry: hydrocarbons from anoxic marine basins, Org. Geochem., 21, 629–644, https://doi.org/10.1016/0146-6380(94)90009-4, 1994.

Grinko, A. A., Goncharov, I. V., Shakhova, N. E., Gustafsson, Ö., Oblasov, N. V., Romankevich, E. A., Zarubin, A. G., Kashapov, R. S., Chernykh, D. V., Gershelis, E. V., Dudarev, O. V., Mazurov, A. K., and Semiletov, I. P.: Sediment organic matter in areas of intense methane release in the Laptev Sea: characteristics of molecular composition, Russ. Geol. Geophys., 61 (4), 456–477, 2020.

605 Grinko, A.A., Gershelis, E.V., Cherykh, D.V., Kurilenko, A.V., Dudarev, O., Kosmach, D.A., and Semiletov, I.P.: Characterization of Organic Matter in Areas of Methane Emission in the Laptev Sea (Expedition 2016). Geochem. Int. 63, 496-509, https://doi.org/10.1134/S0016702924601451, 2025.

Hanson, R. S. and Hanson, T. E.: Methanotrophic Bacteria, MICROBIOLOGICAL REVIEWS, 439–471 pp., 1996.
610
Hinrichs, K.: A molecular recorder of methane hydrate destabilization, Geochemistry, Geophysics, Geosystems, 2, https://doi.org/10.1029/2000gc000118, 2001.

Hinrichs, K., Hmel, L.R., and Sylva, S.P.: Molecular Fossil Record of Elevated Methane Levels in Late Pleistocene Coastal
615 Waters, Science 299 (5610), 1214-1217, https://doi.org/10.1126/science.1079601, 2003.

Holmes, R. M., McClelland, J. W., Peterson, B. J., Tank, S. E., Bulygina, E., Eglinton, T. I., Gordeev, V. V., Gurtovaya, T. Y., Raymond, P. A., Repeta, D. J., Staples, R., Striegl, R. G., Zhulidov, A. V., and Zimov, S. A.: Seasonal and Annual Fluxes of Nutrients and Organic Matter from Large Rivers to the Arctic Ocean and Surrounding Seas, Estuaries and Coasts, 35, 369–
620 382, https://doi.org/10.1007/s12237-011-9386-6, 2012.

Hugelius, G., Ramage, J., Burke, E., Chatterjee, A., Smallman, T. L., Aalto, T., Bastos, A., Biasi, C., Canadell, J. G., Chandra, N., Chevallier, F., Ciais, P., Chang, J., Feng, L., Jones, M. W., Kleinen, T., Kuhn, M., Lauerwald, R., Liu, J., López-Blanco, E., Luijkx, I. T., Marushchak, M. E., Natali, S. M., Niwa, Y., Olefeldt, D., Palmer, P. I., Patra, P. K., Peters, W., Potter, S.,
625 Poulter, B., Rogers, B. M., Riley, W. J., Saunois, M., Schuur, E. A. G., Thompson, R. L., Treat, C., Tsuruta, A., Turetsky, M. R., Virkkala, A. M., Voigt, C., Watts, J., Zhu, Q., and Zheng, B.: Permafrost Region Greenhouse Gas Budgets Suggest a Weak CO_2 Sink and CH_4 and N_2O Sources, But Magnitudes Differ Between Top-Down and Bottom-Up Methods, Global Biogeochem Cycles, 38, https://doi.org/10.1029/2023GB007969, 2024.

630 Inglis, G. N., Naafs, B. D. A., Zheng, Y., Schellekens, J., and Pancost, R. D.: $\delta^{13}C$ values of bacterial hopanoids and leaf waxes as tracers for methanotrophy in peatlands, Geochim Cosmochim Acta, 260, 244–256, https://doi.org/10.1016/j.gca.2019.06.030, 2019.

Jakobsson, M., Mohammad, R., Karlsson, M., Salas-Romero, S., Vacek, F., Heinze, F., Bringensparr, C., Castro, C. F.,
635 Johnson, P., Kinney, J., Cardigos, S., Bogonko, M., Accettella, D., Amblas, D., An, L., Bohan, A., Brandt, A., Bünz, S., Canals, M., Casamor, J. L., Coakley, B., Cornish, N., Danielson, S., Demarte, M., Di Franco, D., Dickson, M. L., Dorschel, B., Dowdeswell, J. A., Dreutter, S., Fremand, A. C., Hall, J. K., Hally, B., Holland, D., Hong, J. K., Ivaldi, R., Knutz, P. C., Krawczyk, D. W., Kristofferson, Y., Lastras, G., Leck, C., Lucchi, R. G., Masetti, G., Morlighem, M., Muchowski, J., Nielsen,

T., Noormets, R., Plaza-Faverola, A., Prescott, M. M., Purser, A., Rasmussen, T. L., Rebesco, M., Rignot, E., Rysgaard, S.,

640 Silyakova, A., Snoeijs-Leijonmalm, P., Sørensen, A., Straneo, F., Sutherland, D. A., Tate, A. J., Travaglini, P., Trenholm, N., van Wijk, E., Wallace, L., Willis, J. K., Wood, M., Zimmermann, M., Zinglersen, K. B., and Mayer, L.: The International Bathymetric Chart of the Arctic Ocean Version 5.0, Scientific Data , 11, https://doi.org/10.1038/s41597-024-04278-w, 2024.

Kusch, S. and Rush, D.: Revisiting the precursors of the most abundant natural products on Earth: A look back at 30+ years

645 of bacteriohopanepolyol (BHP) research and ahead to new frontiers, https://doi.org/10.1016/j.orggeochem.2022.104469, 1 October 2022.

Kannenberg, E.L., Perzl, M., and Härtner, T.: The occurrence of hopanoid lipids in Bradyrhizobium bacteria , FEMS Microbiol Lett, 127, 255–262, https://doi.org/10.1111/j.1574-6968.1995.tb07482.x, 1995.

650

Lindgren, A., Hugelius, G., and Kuhry, P.: Extensive loss of past permafrost carbon but a net accumulation into present-day soils, Nature, 560, 219–222, https://doi.org/10.1038/s41586-018-0371-0, 2018.

Maciute, A., Broman, E., Nascimento, F. J. A., Tesi, T., Yakushev, E., Wild, B., Kirillova, E., Semiletov, I., Gustafsson, Ö.,

655 and Bonaglia, S.: Environmental Gradients, Not Geographic Boundaries, Structure Meiofaunal Communities in Siberian Seas, Environmental DNA, 7, https://doi.org/10.1002/edn3.70124, 2025.

Mackenzie, A.S., Lewis, C.A., and Maxwell, J.R.: Molecular parameters of maturation in the Toarcian shales, Paris Basin, France-IV. Laboratory thermal alteration studies*, Geochim Cosmochim Acta, 45, 2369-2376, https://doi.org/10.1016/0016-

660 7037(81)90090-9, 1981.

Mao, S. H., Zhang, H. H., Zhuang, G. C., Li, X. J., Liu, Q., Zhou, Z., Wang, W. L., Li, C. Y., Lu, K. Y., Liu, X. T., Montgomery, A., Joye, S. B., Zhang, Y. Z., and Yang, G. P.: Aerobic oxidation of methane significantly reduces global diffusive methane emissions from shallow marine waters, Nat Commun, 13, https://doi.org/10.1038/s41467-022-35082-y, 2022.

665

Martens, J., Wild, B., Muschitiello, F., O'regan, M., Jakobsson, M., Semiletov, I., Dudarev, O. V, and Gustafsson, Ö.: Remobilization of dormant carbon from Siberian-Arctic permafrost during three past warming events, Sci. Adv, 6546–6562 pp., 2020.

670 Martens, J., Wild, B., Semiletov, I., Dudarev, O. V., and Gustafsson, Ö.: Circum-Arctic release of terrestrial carbon varies between regions and sources, Nat Commun, 13, https://doi.org/10.1038/s41467-022-33541-0, 2022.

McClelland, J. W., Holmes, R. M., Peterson, B. J., Raymond, P. A., Striegl, R. G., Zhulidov, A. V., Zimov, S. A., Zimov, N., Tank, S. E., Spencer, R. G. M., Staples, R., Gurtovaya, T. Y., and Griffin, C. G.: Particulate organic carbon and nitrogen export from major Arctic rivers, Global Biogeochem Cycles, 30, 629–643, https://doi.org/10.1002/2015GB005351, 2016.

Milkov, A.V., and Etiope, G.: Revised genetic diagrams for natural gases based on a global dataset of >20,000 samples, Org. Geochem, 125, 109-120, https://doi.org/10.1016/j.orggeochem.2018.09.002, 2018.

Nicolsky, D. and Shakhova, N.: Modeling sub-sea permafrost in the East Siberian Arctic Shelf: The dmitry laptev strait, Environmental Research Letters, 5, https://doi.org/10.1088/1748-9326/5/1/015006, 2010.

Obu, J., Westermann, S., Bartsch, A., Berdnikov, N., Christiansen, H. H., Dashtseren, A., Delaloye, R., Elberling, B., Etzelmüller, B., Kholodov, A., Khomutov, A., Kääb, A., Leibman, M. O., Lewkowicz, A. G., Panda, S. K., Romanovsky, V., Way, R. G., Westergaard-Nielsen, A., Wu, T., Yamkhin, J., and Zou, D.: Northern Hemisphere permafrost map based on TTOP modelling for 2000–2016 at 1 km2 scale, https://doi.org/10.1016/j.earscirev.2019.04.023, 1 June 2019.

Overduin, P. P., Schneider von Deimling, T., Miesner, F., Grigoriev, M. N., Ruppel, C., Vasiliev, A., Lantuit, H., Juhls, B., and Westermann, S.: Submarine Permafrost Map in the Arctic Modeled Using 1-D Transient Heat Flux (SuPerMAP), J Geophys Res Oceans, 124, 3490–3507, https://doi.org/10.1029/2018JC014675, 2019.

Ourisson, G., Albrecht, P. & Rohmer, M.: The hopanoids: palaeochemistry and biochemistry of a group of natural products, Pure Appl. Chem. 51, 709–729, https://doi.org/10.1351/pac197951040709, 1979.

Pancost, R. D., Coleman, J. M., Love, G. D., Chatzi, A., Bouloubassi, I., and Snape, C. E.: Kerogen-bound glycerol dialkyl tetraether lipids released by hydropyrolysis of marine sediments: A bias against incorporation of sedimentary organisms?, Org Geochem, 39, 1359–1371, https://doi.org/10.1016/j.orggeochem.2008.05.002, 2008.

Parada, A. E., Needham, D. M., and Fuhrman, J. A.: Every base matters: Assessing small subunit rRNA primers for marine microbiomes with mock communities, time series and global field samples, Environ Microbiol, 18, 1403–1414, https://doi.org/10.1111/1462-2920.13023, 2016.

Parnell, A. C., Phillips, D. L., Bearhop, S., Semmens, B. X., Ward, E. J., Moore, J. W., Jackson, A. L., Grey, J., Kelly, D. J., and Inger, R.: Bayesian stable isotope mixing models, Environmetrics, 24, 387–399, https://doi.org/10.1002/env.2221, 2013.

26

Quast, C., Pruesse, E., Yilmaz, P., Gerken, J., Schweer, T., Yarza, P., Peplies, J., and Glöckner, F. O.: The SILVA ribosomal RNA gene database project: Improved data processing and web-based tools, Nucleic Acids Res, 41, https://doi.org/10.1093/nar/gks1219, 2013.

710 Racolta, S., Juhl, P. B., Sirim, D., and Pleiss, J.: The triterpene cyclase protein family: a systematic analysis, Proteins, 80, 2009–2019, https://doi.org/10.1002/prot.24089, 2012.

Ramage, J., Kuhn, M., Virkkala, A. M., Voigt, C., Marushchak, M. E., Bastos, A., Biasi, C., Canadell, J. G., Ciais, P., López-Blanco, E., Natali, S. M., Olefeldt, D., Potter, S., Poulter, B., Rogers, B. M., Schuur, E. A. G., Treat, C., Turetsky, M. R.,
715 Watts, J., and Hugelius, G.: The Net GHG Balance and Budget of the Permafrost Region (2000–2020) From Ecosystem Flux Upscaling, Global Biogeochem Cycles, 38, https://doi.org/10.1029/2023GB007953, 2024.

Rohmer, M., Dastillung, M., and Ourisson, G. Hopanoids from C30 to C35 in recent muds. Naturwissenschaften 67, 456-458, https://doi.org/10.1007/BF00405643, 1980.

720

Romanovskii, N. N. and Hubberten, H. W.: Results of permafrost modelling of the lowlands and shelf of the Laptev Sea Region, Russia, Permafr Periglac Process, 12, 191–202, https://doi.org/10.1002/ppp.387, 2001.

Romanovskii, N. N., Hubberten, H. W., Gavrilov, A. V., Eliseeva, A. A., and Tipenko, G. S.: Offshore permafrost and gas
725 hydrate stability zone on the shelf of East Siberian Seas, Geo-Marine Letters, 25, 167–182, https://doi.org/10.1007/s00367-004-0198-6, 2005.

Rutz, A., Sorokina, M., Galgonek, J., Mietchen, D., Willighagen, E., Gaudry, A., Graham, J. G., Stephan, R., Page, R., Vondrášek, J., Steinbeck, C., Pauli, G. F., Wolfender, J. L., Bisson, J., and Allard, P. M.: The LOTUS initiative for open
730 knowledge management in natural products research, Elife, 11, https://doi.org/10.7554/eLife.70780, 2022.

Salvadó, J. A., Tesi, T., Sundbom, M., Karlsson, E., Krusä, M., Semiletov, I. P., Panova, E., and Gustafsson, Ö.: Contrasting composition of terrigenous organic matter in the dissolved, particulate and sedimentary organic carbon pools on the outer East Siberian Arctic Shelf, Biogeosciences, 13, 6121–6138, https://doi.org/10.5194/bg-13-6121-2016, 2016.

735

Samylina, O. S., Rusanov, I. I., Tarnovetskii, I. Y., Yakushev, E. V., Grinko, A. A., Zakharova, E. E., Merkel, A. Y., Kanapatskiy, T. A., Semiletov, I. P., and Pimenov, N. V.: On the Possibility of Aerobic Methane Production by Pelagic Microbial Communities of the Laptev Sea, Microbiology (Russian Federation), 90, 145–157, https://doi.org/10.1134/S0026261721020119, 2021.

740

Sapart, C. J., Shakhova, N., Semiletov, I., Jansen, J., Szidat, S., Kosmach, D., Dudarev, O., Van Der Veen, C., Egger, M., Sergienko, V., Salyuk, A., Tumskoy, V., Tison, J. L., and Röckmann, T.: The origin of methane in the East Siberian Arctic Shelf unraveled with triple isotope analysis, Biogeosciences, 14, 2283–2292, https://doi.org/10.5194/bg-14-2283-2017, 2017.

Saunois, M., Martinez, A., Poulter, B., Zhang, Z., Raymond, P. A., Regnier, P., Canadell, J. G., Jackson, R. B., Patra, P. K.,
745 Bousquet, P., Ciais, P., Dlugokencky, E. J., Lan, X., Allen, G. H., Bastviken, D., Beerling, D. J., Belikov, D. A., Blake, D. R., Castaldi, S., Crippa, M., Deemer, B. R., Dennison, F., Etiope, G., Gedney, N., Höglund-Isaksson, L., Holgerson, M. A., Hopcroft, P. O., Hugelius, G., Ito, A., Jain, A. K., Janardanan, R., Johnson, M. S., Kleinen, T., Krummel, P. B., Lauerwald, R., Li, T., Liu, X., Mcdonald, K. C., Melton, J. R., Mühle, J., Müller, J., Murguia-Flores, F., Niwa, Y., Noce, S., Pan, S., Parker, R. J., Peng, C., Ramonet, M., Riley, W. J., Rocher-Ros, G., Rosentreter, J. A., Sasakawa, M., Segers, A., Smith, S. J.,
750 Stanley, E. H., Thanwerdas, J., Tian, H., Tsuruta, A., Tubiello, F. N., Weber, T. S., Van Der Werf, G. R., Worthy, D. E. J., Xi, Y., Yoshida, Y., Zhang, W., Zheng, B., Zhu, Q., Zhu, Q., and Zhuang, Q.: Global Methane Budget 2000-2020, Earth Syst Sci Data, 17, 1873–1958, https://doi.org/10.5194/essd-17-1873-2025, 2025.

Savvichev, A. S., Rusanov, I. I., Kadnikov, V. V., Beletsky, A. V., Zakcharova, E. E., Samylina, O. S., Sigalevich, P. A.,
755 Semiletov, I. P., Ravin, N. V., and Pimenov, N. V.: Biogeochemical Activity of Methane-Related Microbial Communities in Bottom Sediments of Cold Seeps of the Laptev Sea, Microorganisms, 11, https://doi.org/10.3390/microorganisms11020250, 2023.

Schaeffer, R., Schipper, E. L. F., Ospina, D., Mirazo, P., Alencar, A., Anvari, M., Artaxo, P., Biresselioglu, M. E., Blome, T.,
760 Boeckmann, M., Brink, E., Broadgate, W., Bustamante, M., Cai, W., Canadell, J. G., Cardinale, R., Chidichimo, M. P., Ditlevsen, P., Eicker, U., Feron, S., Fikru, M. G., Fuss, S., Gaye, A. T., Gustafsson, Ö., Harring, N., He, C., Hebden, S., Heilemann, A., Hirota, M., Janardhanan, N., Juhola, S., Jung, T. Y., Kejun, J., Kilkiş, Ş., Kumarasinghe, N., Lapola, D., Lee, J. Y., Levis, C., Lusambili, A., Maasakkers, J. D., MacIntosh, C., Mahmood, J., Mankin, J. S., Marchegiani, P., Martin, M., Mukherji, A., Muñoz-Erickson, T. A., Niazi, Z., Nyangon, J., Pandipati, S., Perera, A. T. D., Persad, G., Persson, Å., Redman,
765 A., Riipinen, I., Rockström, J., Roffe, S., Roy, J., Sakschewski, B., Samset, B. H., Schlosser, P., Sharifi, A., Shih, W. Y., Sioen, G. B., Sokona, Y., Stammer, D., Suk, S., Thiam, D., Thompson, V., Tullos, E., van Westen, R. M., Vargas Falla, A. M., Vecellio, D. J., Worden, J., Wu, H. C., Xu, C., Yang, Y., Zachariah, M., Zhang, Z., and Ziervogel, G.: Ten new insights in climate science 2024, https://doi.org/10.1016/j.oneear.2025.101285, 20 June 2025.

770 Schwartz-Narbonne, R., Schaeffer, P., Lengger, S. K., Blewett, J., Martin Jones, D., Motsch, E., Crombie, A., Jetten, M. S. M., Mikkelsen, D., Normand, P., Nuijten, G. H. L., Pancost, R. D., and Rush, D.: Bacterial physiology highlighted by the δ13C fractionation of bacteriohopanetetrol isomers, Org Geochem, 181, https://doi.org/10.1016/j.orggeochem.2023.104617, 2023.

Semiletov, I. P.: Aquatic Sources and Sinks of CO 2 and CH 4 in the Polar Regions, Journal of the Atmospheric Sciences

775   56(2), 286-306, https://doi.org/10.1175/1520-0469(1999)056%3C0286:ASASOC%3E2.0.CO;2, 1999.

Sessions, A. L., Zhang, L., Welander, P. V, Doughty, D., Summons, R. E., and Newman, D. K.: Identification and quantification of polyfunctionalized hopanoids by high temperature gas chromatography-mass spectrometry, 2013.

780   Shakhova, N., Semiletov, I., Salyuk, A., Yusupov, V., Kosmach, D., and Gustafsson, Ö.: Extensive Methane Venting to the Atmosphere   from   Sediments   of   the   East   Siberian   Arctic   Shelf,   Science   327   (5970),   1246-1250, https://doi.org/10.1126/science.1182221, 2010.

Shakhova, N. and Semiletov, I.: Methane release and coastal environment in the East Siberian Arctic shelf, Journal of Marine

785   Systems, 66, 227–243, https://doi.org/10.1016/j.jmarsys.2006.06.006, 2007.

Shakhova, N., Semiletov, I., Leifer, I., Sergienko, V., Salyuk, A., Kosmach, D., Chernykh, D., Stubbs, C., Nicolsky, D., Tumskoy, V., and Gustafsson, Ö.: Ebullition and storm-induced methane release from the East Siberian Arctic Shelf, Nat Geosci, 7, 64–70, https://doi.org/10.1038/ngeo2007, 2014.

790

Shakhova, N., Semiletov, I., Sergienko, V., Lobkovsky, L., Yusupov, V., Salyuk, A., Salomatin, A., Chernykh, D., Kosmach, D., Panteleev, G., Nicolsky, D., Samarkin, V., Joye, S., Charkin, A., Dudarev, O., Meluzov, A., and Gustafsson, Ö.: The East Siberian Arctic Shelf: towards further assessment of permafrost-related methane fluxes and role of sea ice, Philos. Trans. R. Soc. A, 373, 20140451, https://doi.org/10.1098/rsta.2014.0451, 2015.

795

Shakhova, N., Semiletov, I., Gustafsson, O., Sergienko, V., Lobkovsky, L., Dudarev, O., Tumskoy, V., Grigoriev, M., Mazurov, A. K., Salyuk, A., Ananiev, R., Koshurnikov, A., Kosmach, D., Charkin, A., Dmitrevsky, N., Karnaukh, V., Gunar, A., Meluzov, A., and Chernykh, D.: Current rates and mechanisms of subsea permafrost degradation in the East Siberian Arctic Shelf, Nat Commun, 8, https://doi.org/10.1038/ncomms15872, 2017.

800

Shakhova, N., Semiletov, I., and Chuvilin, E.: Understanding the Permafrost–Hydrate System and Associated Methane Releases in the East Siberian Arctic Shelf, Geosciences, 9(6), 251, https://doi.org/10.3390/geosciences9060251, 2019.

Sinninghe Damsté, J. S., Rijpstra, W. I. C., Schouten, S., Fuerst, J. A., Jetten, M. S. M., and Strous, M.: The occurrence of

805   hopanoids in planctomycetes: Implications for the sedimentary biomarker record, Org Geochem, 35, 561–566, https://doi.org/10.1016/j.orggeochem.2004.01.013, 2004.

Sinninghe Damsté, J. S., Schouten, S., and Volkman, J. K.: C27-C30 neohop-13(18)-enes and their saturated and aromatic derivatives in sediments: Indicators for diagenesis and water column stratification, Geochim Cosmochim Acta, 133, 402–421, https://doi.org/10.1016/j.gca.2014.03.008, 2014.

Sohlenkamp, C. and Geiger, O.: Bacterial membrane lipids: Diversity in structures and pathways, https://doi.org/10.1093/femsre/fuv008, 5 September 2015.

Steinbach, J., Holmstrand, H., Shcherbakova, K., Kosmach, D., Brüchert, V., Shakhova, N., Salyuk, A., Sapart, C. J., Chernykh, D., Noormets, R., Semiletov, I., and Gustafsson, Ö.: Source apportionment of methane escaping the subsea permafrost system in the outer Eurasian Arctic Shelf, https://doi.org/10.1073/pnas.2019672118/-/DCSupplemental, 2021.

Stepanova, S. V., Polukhin, A. A., and Kostyleva, A. V.: Hydrochemical structure of the waters in the eastern part of the Laptev Sea in autumn 2015, Oceanology (Wash D C), 57, 58–64, https://doi.org/10.1134/S0001437017010180, 2017.

Summons, R. E., Jahnke, L. L., and Roksandic, Z.: Carbon isotopic fractionation in lipids from methanotrophic bacteria: Relevance for interpretation of the geochemical record of biomarkers, Geochimica et Cosmochimica Acta, 2853–2863, https://doi.org/10.1016/0016-7037(94)90119-8, 1994.

Summons, R. E., Jahnke, L. L., Hope, J.M., and Logan, G.A.: 2-Methylhopanoids as biomarkers for cyanobacterial oxygenic photosynthesis, Nature 400, 554-557, https://doi.org/10.1038/23005, 1999.

Sun, F., Hu, W., Cao, J., Wang, X., Zhang, Z., Ramezani, J., and Shen, S.: Sustained and intensified lacustrine methane cycling during Early Permian climate warming, Nat Commun, 13, https://doi.org/10.1038/s41467-022-32438-2, 2022.

Takeuchi, M., Katayama, T., Yamagishi, T., Hanada, S., Tamaki, H., Kamagata, Y., Oshima, K., Hattori, M., Marumo, K., Nedachi, M., Maeda, H., Suwa, Y., and Sakata, S.: Methyloceanibacter caenitepidi gen. nov., sp. nov., a facultatively methylotrophic bacterium isolated from marine sediments near a hydrothermal vent, Int J Syst Evol Microbiol, 64, 462–468, https://doi.org/10.1099/ijs.0.053397-0, 2014.

Takeuchi, M., Ozaki, H., Hiraoka, S., Kamagata, Y., Sakata, S., Yoshioka, H., and Iwasaki, W.: Possible cross-feeding pathway of facultative methylotroph Methyloceanibacter caenitepidi Gela4 on methanotroph Methylocaldum marinum S8, PloS One, 14, https://doi.org/10.1371/journal.pone.0213535, 2019.

Thornton, B., Geibel, M.C., Crill, P.M., Humborg, C., and Mörth, C.M: Methane fluxes from the sea to the atmosphere across the Siberian shelf seas, Geophys. Res. Lett. 43, 5869-5877, https://doi.org/10.1002/2016GL068977, 2016.

Thornton, B., Prytherch, J., Anderson, K., Brooks, I.M., Salisbury, D., Tjernström, M., and Crill, P.M.: Shipborne eddy covariance observations of methane fluxes constrain Arctic sea emissions, Science Advances, 6(5), eaay7934, https://doi.org/10.1126/sciadv.aay7934, 2020.

Tikhonova, E. N., Kadnikov, V. V., Rusanov, I. I., Beletsky, A. V., Zakharova, E. E., Samylina, O. S., Ravin, N. V., and Pimenov, N. V.: Methane-Oxidizing Activity and Phylogenetic Diversity of Aerobic Methanotrophs in the Laptev Sea Upper Sediment Horizons, Microbiology (Russian Federation), 90, 314–323, https://doi.org/10.1134/S0026261721030127, 2021.

van Dongen, B. E., Semiletov, I., Weijers, J. W. H., and Gustafsson, Ö.: Contrasting lipid biomarker composition of terrestial organic matter exported from across the Eurasian Arctic by the five great Russian Arctic rivers, Global Biogeochem Cycles, 22, https://doi.org/10.1029/2007GB002974, 2008.

van Winden, J. F., Talbot, H. M., Reichart, G. J., McNamara, N. P., Benthien, A., and Sinninghe Damsté, J. S.: Influence of temperature on the δ13C values and distribution of methanotroph-related hopanoids in Sphagnum-dominated peat bogs, Geobiology, 18, 497–507, https://doi.org/10.1111/gbi.12389, 2020.

Vekeman, B., Kerckhof, F.-M., Cremers, G., De Vos, P., Vandamme, P., Boon, N., Op Den Camp, H. J. M., and Heylen, K.: New Methyloceanibacter diversity from North Sea sediments includes methanotroph containing solely the soluble methane monooxygenase, Environ. Microbiol., 18, 4523–4536, 2016.

Vonk, J. E., Sanchez-Garca, L., Van Dongen, B. E., Alling, V., Kosmach, D., Charkin, A., Semiletov, I. P., Dudarev, O. V., Shakhova, N., Roos, P., Eglinton, T. I., Andersson, A., and Gustafsson, A.: Activation of old carbon by erosion of coastal and subsea permafrost in Arctic Siberia, Nature, 489, 137–140, https://doi.org/10.1038/nature11392, 2012.

Wild, B., Shakhova, N., Dudarev, O., Ruban, A., Kosmach, D., Tumskoy, V., Tesi, T., Grimm, H., Nybom, I., Matsubara, F., Alexanderson, H., Jakobsson, M., Mazurov, A., Semiletov, I., and Gustafsson, Ö.: Organic matter composition and greenhouse gas production of thawing subsea permafrost in the Laptev Sea, Nat Commun, 13, https://doi.org/10.1038/s41467-022-32696-0, 2022.

Wittig, S., Berchet, A., Pison, I., Saunois, M., and Paris, J. D.: Surface networks in the Arctic may miss a future methane bomb, Atmos Chem Phys, 24, 6359–6373, https://doi.org/10.5194/acp-24-6359-2024, 2024.

875 Xie, L., Yakushev, E., Semiletov, I., Grinko, A., Gangnus, I., Berezina, A., Osadchiev, A., Zhdanov, I., Polukhin, A., Moiseeva, J., Purgina, D., Pipko, I., Pugach, S., Dudarev, O., and Ge, Z.: Biogeochemical structure of the Laptev Sea in 2015-2020 associated with the River Lena plume, Front. Mar. Sci. 10, 1180054, https://doi.org/10.3389/fmars.2023.1180054, 2023.

Yan, X., Liu, J., Kang, W., Huang, X., Zhou, A., Chen, L., Zhang, J., Dong, H., Chen, Z., Wu, J., Holmstrand, H., Rühland,
880 K. M., Smol, J. P., Chen, F., and Gustafsson, Ö.: Pronounced methane cycling in northern lakes coincided with a rapid rise in atmospheric CH_4 during the last deglacial warming, Sci. Adv., 11 (29), eadt2561, https://doi.org/10.1126/sciadv.adt2561, 2025.